Palaeontology
The Palaeontological Association
www.palass.org

[Palaeontology, Vol. 58, Part 4, 2015, pp. 723–742]

THE SKULL AND ENDOCRANIUM OF A LOWER JURASSIC ICHTHYOSAUR BASED ON DIGITAL RECONSTRUCTIONS

by RYAN D. MAREK[1], BENJAMIN C. MOON[1], MATT WILLIAMS[2] *and* MICHAEL J. BENTON[1]*

[1]School of Earth Sciences, Life Sciences Building, University of Bristol, Tyndalls Avenue, Bristol, BS8 1TQ, UK; e-mails: ryan.marek.2010@my.bristol.ac.uk, benjamin.moon@bristol.ac.uk, mike.benton@bristol.ac.uk
[2]Bath Royal Literary and Scientific Institution, 16–18 Queen Square, Bath, BA1 2HN, UK; e-mail: matt.williams@brlsi.org
*Corresponding author

Typescript received 6 February 2015; accepted in revised form 27 April 2015

Abstract: Even after 200 years of study, some details of the cranial anatomy of ichthyosaurs, one of the most successful groups of marine vertebrates in the Mesozoic, are still unclear. New information on the braincase, palate and occiput are provided from three-dimensional scans of an exceptionally preserved ichthyosaur (‘*Hauffiopteryx*’ *typicus*) skull from the Toarcian (183–174 Ma, Lower Jurassic) of Strawberry Bank, England. This ichthyosaur has unusual, hollow, tubular hyoid bars. The occipital and braincase region is fully reconstructed, creating the first digital cranial endocast of an ichthyosaur. Enlarged optic lobes and an enlarged cerebellum suggest neuroanatomical adaptations that allowed it to be a highly mobile, visual predator. The olfactory region also appears to be enlarged, suggesting that olfaction was more important for ichthyosaurs than has been assumed. Phylogenetic analysis suggests this ichthyosaur is closely related to, but distinct from, *Hauffiopteryx*, and positioned within Thunnosauria, a more derived position than previously recovered. These results further our knowledge of ichthyosaur cranial anatomy in three dimensions and provide a platform in which to study the anatomical adaptations that allowed ichthyosaurs to dominate the marine realm during the Mesozoic.

Key words: Ichthyosauria, Leptonectidae, Lower Jurassic, Lias, systematics, neurobiology.

ICHTHYOSAURS were a group of highly derived diapsid reptiles adapted exclusively to the marine realm (Motani 2005). They were an important component of the marine ecosystem through much of the Mesozoic (Motani 2005), becoming extinct in the early part of the Late Cretaceous (Bardet 1992). During the Triassic, ichthyosaurs had a high diversity and disparity, occupying numerous niches, such as the small, semi-durophagous mixosaurids, the larger predatory *Thalattoarchon* and *Cymbospondylus*, and the massive *Shastasaurus* and *Shonisaurus* (Massare 1987; Fröbisch *et al.* 2013; Motani *et al.* 2013). However, post-Triassic ichthyosaurs greatly reduced their disparity, despite initially retaining similar levels of diversity (Thorne *et al.* 2011). Most post-Triassic ichthyosaurs belong to the clade Thunnosauria, with *Hauffiopteryx typicus* recovered as the immediate out-group to this clade (Fischer *et al.* 2013). Therefore, this species is an important marker in the transition to the great majority of advanced ichthyosaurs.

Most Lower Jurassic ichthyosaur specimens are preserved in flattened and compressed form. This is especially true of exceptionally preserved specimens from Holzmaden, southern Germany (Toarcian, Lower Jurassic), which may show soft tissues and body outlines, but the skeletons are flattened and conceal details, especially within the skull. Other ichthyosaurs may be three dimensional, but disarticulated. The Strawberry Bank deposit in Ilminster, Somerset, UK, has yielded an exceptional fauna of largely three-dimensional and articulated fossils, including insects, cephalopods, fishes, the crocodilian *Pelagosaurus* (Pierce and Benton 2006) and ichthyosaurs previously referred to *Hauffiopteryx* and *Stenopterygius* (Caine and Benton 2011). The deposit is similar in age to the Posidonia Shale of Holzmaden, south-western Germany, being dated as early Toarcian (Moore 1866; Duffin 1978, 1979; Pierce and Benton 2006; Thorne *et al.* 2011). As an initial study, we scanned one ichthyosaur specimen, BRLSI M1399, which was originally assigned to *Hauffiopteryx typicus* Maisch, 2008, by Caine and Benton (2011). The genus *Hauffiopteryx*, with one species, *H. typicus*, has been difficult to place phylogenetically. Maisch (2008) identified it as a basal member of the

doi: 10.1111/pala.12174

Stenopterygiidae, but it was later tentatively assigned simply to basal Thunnosauria by Caine and Benton (2011). The aim of this study was to present a comprehensive reconstruction of the skull of a single ichthyosaur specimen, presenting all anatomical details, and focusing on those areas, such as braincase, occiput and palate that are rarely available for study.

Many three-dimensionally preserved crania of various groups of organisms have been analysed using computed tomographic (CT) imaging since the early 2000s, with the practice becoming commonplace in palaeontological literature. To date, these techniques have given insight into the cranial function and anatomy of many taxa, ranging from dinosaurs (Rayfield 2005; Lautenschlager *et al.* 2012, 2013; Cuff and Rayfield 2013) to sabre-toothed cats (Wroe *et al.* 2013). They also give much needed information on important neuroanatomical transitions, as in the evolution of the avian brain (Balanoff *et al.* 2013). Yet to date, these techniques have not been fully applied to ichthyosaurs, except in some descriptive anatomical studies (McGowan 1989; Kear 2005), and only recently have been applied to other marine reptiles (Fernández *et al.* 2011; Sato *et al.* 2011; Neenan and Scheyer 2012; Araújo and Polcyn 2013; Herrera *et al.* 2013; Foffa *et al.* 2014*a*, *b*). Thus, the exceptional 3D preservation of BRLSI M1399, in conjunction with CT imaging, provides a unique and unprecedented opportunity to explore ichthyosaur sensory biology and neuroanatomy, an area previously occupied by little more than rubber casts and speculation.

Institutional abbreviation. BRLSI, Bath Royal Literary and Scientific Institution, Queen's Square, Bath, UK.

MATERIALS AND METHODS

The Strawberry Bank collection includes eight specimens of ichthyosaurs, previously assigned to the species *Hauffiopteryx typicus* and *Stenopterygius triscissus*. For this study, we selected a three-dimensionally preserved skull, BRLSI M1399 (Fig. 1), for study. This material was described by Caine and Benton (2011, pp. 1080–1081, figs 8, 9, 12), but has since been prepared further. It is thought to be a juvenile individual, based on its small size and allometric differences from close relatives, with a total skull length of 348 mm. BRLSI M3199 is preserved in a limestone concretion.

The skull was CT-scanned in a custom-designed Nikon/Metris 225 kB/450 kV hutch using a 1-pixel-wide detector at the Multiscale, Microtomographic Volume Imaging Unit at the University of Southampton, UK. Scan parameters were set at 280 kV, 539 μA, no filter, 160 μm pixel size, 90-ms exposure time per projection, 1701 projections with one frame per projection and the detector was binned two times. The data files were then imported into Avizo (initially version 6.3.1, later transported to versions 7.0 and 8.0, Visualization Science Group), running on HP Workstations with 16 and 72 GB of RAM, using Windows XP SP2 and Windows 7, respectively. The bones of the skull were individually separated and highlighted using Avizo segmentation editor. Three-dimensional surface models and volumes were then made to visualise these bones.

When creating the digital endocast, damage on the left side of the skull and braincase was repaired by mirroring the corresponding elements from the right side of the skull, following procedures described by Lautenschlager (2014). Mirrored elements were the prootic, opisthotic, quadrate, supratemporal, squamosal, parietal and postfrontal. All elements were then extracted as a single surface. The endocast was created by highlighting the space between these elements, using the same segmentation editors as before.

For phylogenetic analysis, we added BRLSI M1399 as a new terminal taxon to a modified version of the data matrix of Fischer *et al.* (2013). Cranial and postcranial material was scored based on personal observation and the description of Caine and Benton (2011). The coding for *Hauffiopteryx typicus* was completed anew based only upon Belgian and German specimens, as the original coding had incorporated the Bath material. The states for other taxa in this matrix were re-examined and found to be correct (but see note in Marek *et al.* 2015). A parsimony analysis of the matrix was carried out in TNT version 1.1 (Goloboff *et al.* 2008), using implicit enumeration (exact search). Characters were not weighted and, aside from characters 20, 39, 49 and 57, were not ordered (as in Fischer *et al.* 2013). Bremer and symmetrical resampling (10 000 replicates, removal probability 33%; Goloboff *et al.* 2003) support values were calculated in TNT. New character codings can be found in Marek *et al.* (2015).

DESCRIPTION

The external skull anatomy of BRLSI M1399 has been described previously by Caine and Benton (2011) and is largely corroborated by our observations. Therefore, we describe only the internal morphology and new features below. Caine and Benton (2011) concluded that this specimen represented a juvenile, with many skull elements not fully fused, and a skull length of less than 400 mm, much smaller than close relatives from Germany (McGowan 1973). Fusion of the basisphenoid and the parasphenoid to form the parabasisphenoid has been suggested as an indicator of osteological maturity in other parvipelvians,

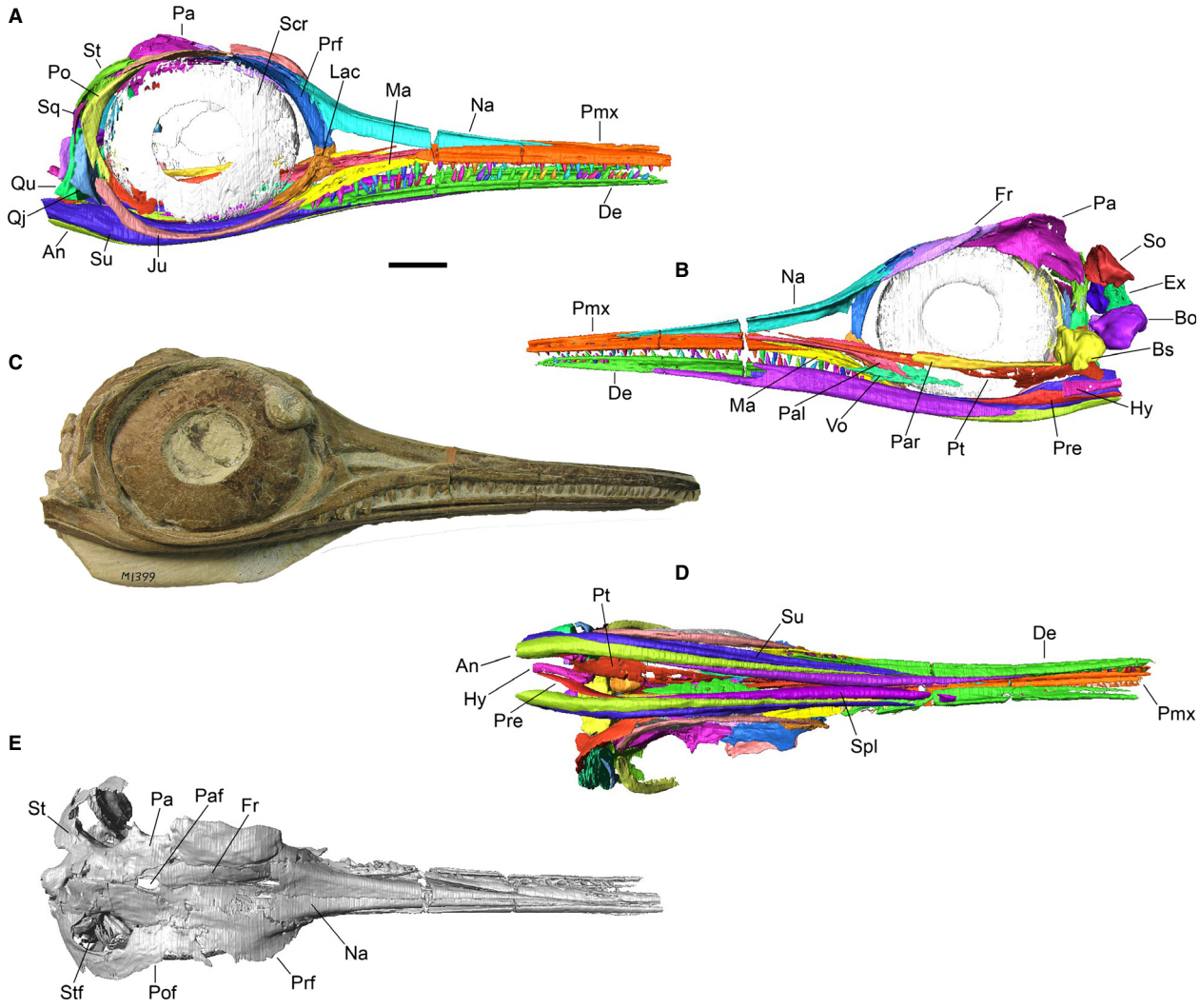

FIG. 1. Skull of BRLSI M1399 in right lateral (A, C), medial (B), ventral (D) and dorsal views (E). *Abbreviations*: An, angular; Bs, basisphenoid; De, dentary; Fr, frontal; Hy, hyoid; Ju, jugal; Lac, lacrimal; Max, maxilla; Na, nasal; Pa, parietal; Paf, parietal foramen; Pal, palatine; Par, parasphenoid; Prf, prefrontal; Pmx, premaxilla; Po, postorbital; Pof, postfrontal; Pt, pterygoid; Qj, quadratojugal; Qu, quadrate; Scr, sclerotic ring; Spl, splenial; Sq, squamosal; St, supratemporal; Stf, supratemporal fenestra; Su, surangular; Vo, vomer. Scale bar represents 20 mm. Colour online.

such as *Platypterygius australis* and *Sveltonectes insolitus* (Kear 2005; Fischer *et al.* 2011), and this is found in BRLSI M1399. This would suggest that BRLSI M1399 is a late-stage juvenile.

Cranium

Premaxilla. The premaxilla (Figs 1A, B, C, 2E, F) is a long, straight element that makes up approximately two-thirds of the length of the rostrum, meeting the other premaxilla medially along most of its length. The medial surface of the premaxilla (Fig. 1C) shows a prominent ridge that runs from the anteriormost tip and becomes narrower posteriorly as it diverges laterally with backward expansion of the rostrum diameter. A deep groove runs longitudinally on the lateral surface (Fig. 1A), becoming shallower and narrower anteriorly, reducing to three small foramina at the anterior end. The alveolar groove is present along the entire length of the premaxilla (Fig. 2F), narrowing anteriorly. The posterior portion of the premaxilla bifurcates (Fig. 2E, F), forming two narrow projections that are deflected laterally and medially below the external nares, the medial projection being longer. There is no supranarial process, as in *Ichthyosaurus* and *Ophthalmosaurus* (McGowan 1973; Kirton 1983). Here, the premaxilla meets, and surrounds, the anterior portion of the maxilla. Both premaxillae are in contact along their

ventromedial margins. The premaxilla also contacts the nasal dorsomedially.

Maxilla. The maxilla (Figs 1A, B, C, 2A–D) is a small element, curving posteroventrally, and with the anterior and posterior tips are overlapped in lateral view (Fig. 1A) by the premaxilla anteriorly, and jugal and lacrimal posteriorly. The highest point is at the approximate mid-point of the element, and the maxilla decreases in height and width both anteriorly and posteriorly. The dorsal surface (Fig. 2C) slopes laterally towards the posterior end, and anteriorly, there is a slight medial slope. Both lateral and medial surfaces are vertical, but the medial surface begins to slope ventrolaterally towards the posterior end. The ventral surface (Fig. 2D) is occupied entirely by the alveolar groove, continuing from the premaxilla, and it narrows backwards.

Nasal. The nasal (Figs 1A, B, D, E, 2G) forms both the posterior portion of the dorsal surface of the rostrum and the anterior portion of the skull roof. This elongate, narrow element ascends posteriorly over the orbit. Laterally (Figs 1A, 2G), the nasal curves ventrally, and this curvature sharpens posteriorly, almost forming a right angle. Internally (Fig. 1B), the surface is concave, oriented horizontally in the posterior portion, and twisting to the vertical towards the front. These two surfaces are separated by a diagonal ridge that terminates posteriorly on the lateral surface, where the nasal forms a broad contact with the prefrontal. The dorsal surface (Fig. 1E) is convex, extends forwards and narrows to a point. The nasals are fused medially along a slightly serrated suture, with only the anteriormost portion unfused (Fig. 1E).

Lacrimal. The 'T-shaped' (Caine and Benton 2011, p. 1080) lacrimal (Figs 1A, 3A–D) forms the anteroventral orbital margin. In lateral view (Fig. 3A), the lacrimal narrows posteriorly, and in dorsal view (Fig. 3C), it narrows to a point anteriorly. This forms a wide, flat and shelf-like orbital margin, which bears a ridge that terminates abruptly where the lacrimal ascends; this may be an artefact of preservation. McGowan (1973) identified a similar ridge in *Ichthyosaurus.* This anterior section of the lateral surface slopes vertically. The medial surface (Fig. 3B) is smoother, with a less prominent ridge emerging on the posterior half of the surface, and two anterodorsally orientated grooves, the anteriormost being the deepest. The posterior portion of the dorsal margin (Fig. 3C) is a smooth concave curve, while the curvature of the anterior portion is more angular. Ventrally (Fig. 3D), the lacrimal is smooth and convex and narrows to a point posteriorly.

Jugal. The J-shaped jugal (Fig. 3E, F) is long, narrow, curved element that forms the ventral border of the orbit, overlapping the posterior portion of the maxilla, and with the posterior portion ascending to meet the postorbital

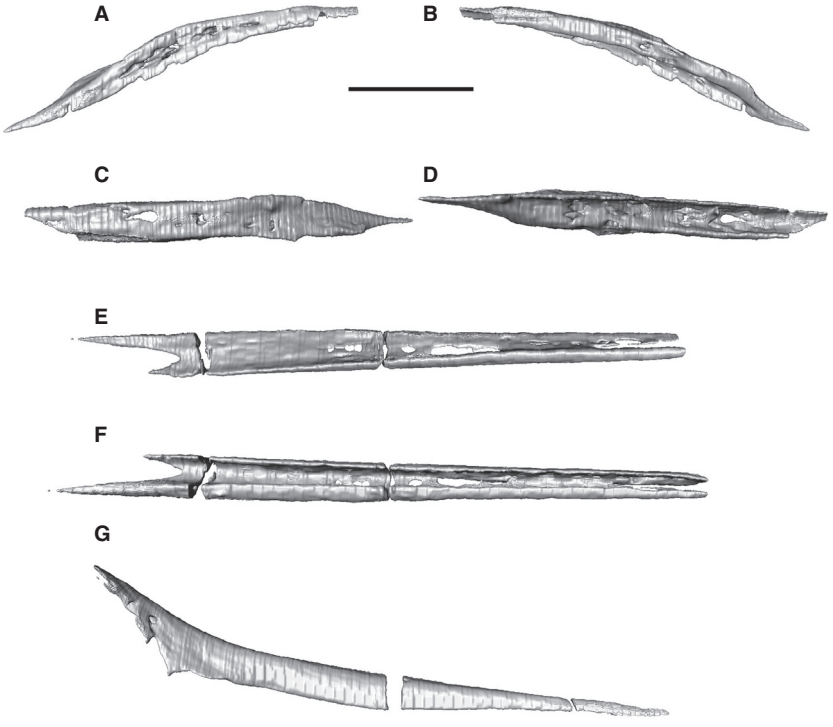

FIG. 2. Elements of the rostrum of BRLSI M1399. A–D, right maxilla in lateral (A), medial (B), dorsal (C) and ventral (D) views. E–F, right premaxilla in dorsal (E) and ventral (F) views. G, right nasal in lateral views. Scale bar represents 20 mm.

and the quadratojugal. This posterior portion is laterally flattened compared to the rest of the element, which becomes anteroventrally flattened in midsection. Posteriorly, the jugal terminates in a rounded, but laterally flattened, edge, while the anterior end terminates in a point (Fig. 3E, F).

Prefrontal. The arched prefrontal (Fig. 4) forms the anterodorsal portion of the orbit margin. It is narrow and flat posteriorly, where it is overlapped by the postfrontal and parietal, becoming wider and thicker anteriorly, terminating in a point where it is overlapped by the lacrimal. At the narrowest point of the dorsal roof (Fig. 4A), a deep, V-shaped anteroposterior groove emerges and steepens further forwards. The ventral surface (Fig. 4B) shows the ridge that divides the dorsal portion from the prefrontal portion that forms part of the orbital margin. In anterior view (Fig. 4C), the prefrontal is vertical, marking the boundary of the orbit and the proximal base of the rostrum.

Frontal. The frontals (Figs 1B, E, 4) form the anteriormost section of the skull roof. The frontal is thickest posteriorly, where it borders the parietal foramen, and thins anteriorly towards the contact with the nasal. The frontal is convex and horizontal around the parietal foramen, and slopes ventrally, with increasing curvature anteriorly, and then flattening into the root of the rostrum. In ventral view (Fig. 4B), the internal frontal crests splay slightly in front of the parietal foramen, and curve together, and then apart anteriorly. The frontals meet each other medially along a straight contact, which becomes interdigitating towards the parietal foramen.

Parietal. The parietals (Figs 1A, B, E, 4) meet medially along a straight contact, up to the parietal foramen, where their anterior tips are separated by the frontals. In dorsal view (Fig. 4A), the parietals are seen to be considerably larger than the frontals. They are broad elements and include posterior processes that meet the supratemporals, then form the medial margin of the supratemporal

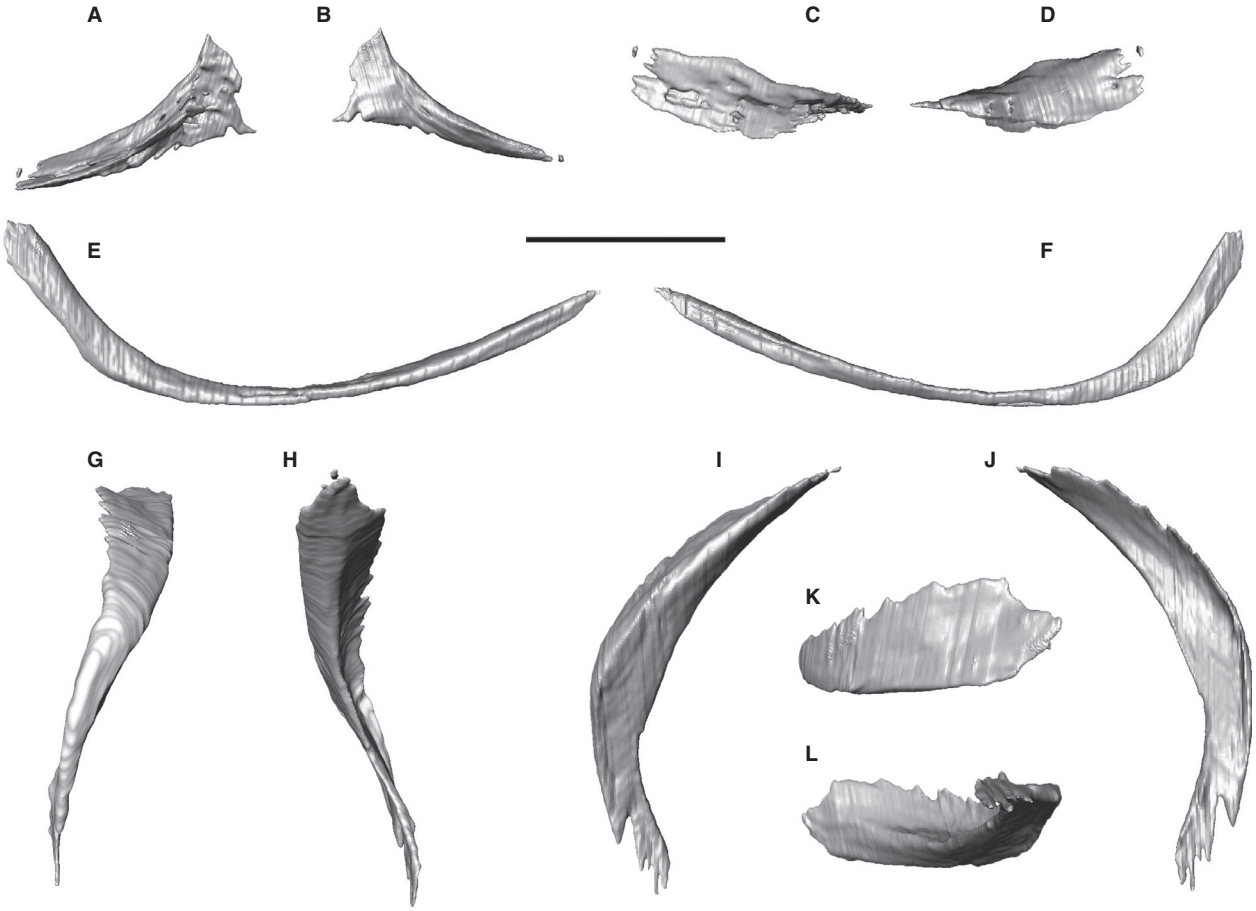

FIG. 3. Orbital components of BRLSI M1399. A–D, right lacrimal in lateral (A), medial (B), dorsal (C) and ventral (D) views. E–F, right jugal in lateral (E) and medial (F) views. G–L, right postorbital in posterior (G), anterior (H), lateral (I), medial (J), dorsal (K) and ventral (L) views. Scale bar represents 20 mm.

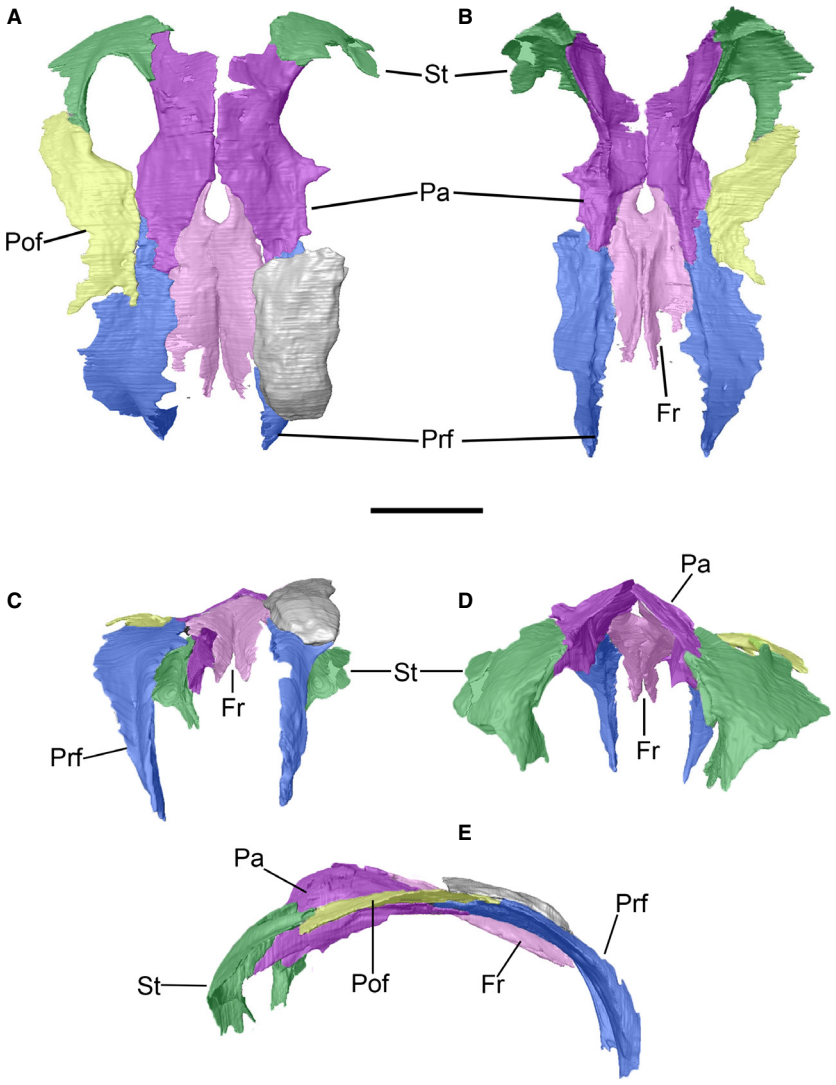

FIG. 4. Skull roof of BRLSI M1399 in dorsal (A), ventral (B), anterior (C), posterior (D) and lateral (E) views. *Abbreviations*: Fr, frontal; Pa, parietal; Pof, postfrontal; Prf, prefrontal; St, supratemporal. Scale bar represents 20 mm. Colour online.

fenestra and run to a point between frontals and prefrontals. In lateral view (Fig. 4E), the parietal is arched, with the highest point at mid-length. In ventral view (Fig. 4B), the surface is concave, with a curved ridge extending from the lateral margin where the posterior process meets the supratemporal, round the margin of the supratemporal fenestra, and extending anteriorly and slightly laterally to join the longitudinal ventral ridge beneath the prefrontal.

Postfrontal. The dorsomedial portion of the orbit is formed by the postfrontal (Figs 1E, 4A, B, E), of which only the right one is preserved in BRLSI M1399. Viewed laterally (Fig. 4E), the postfrontal is a thin, slightly arched element that is thickest at its medial edge. From above (Fig. 4A), the posterior portion is rounded, while the anteriormost portion of the postfrontal splits into two processes that wrap around and overlap the prefrontal. Numerous shallow foramina are present on the dorsal surface. The medial edge is approximately straight in contact with prefrontal and parietal, and then, it curves around the anterior margin of the supratemporal fenestra.

Postorbital. The crescentic postorbital (Figs 1A, C, 3G–L) forms the posterodorsal and posteriormost border of the orbit. In lateral view (Fig. 1A, C), the thickest section of the postorbital is the midsection, and it narrows anteriorly to contact the postfrontal and posteriorly to contact the quadratojugal. Viewed posteriorly (Fig. 3G), the postorbital shows a horizontal dorsal surface and a vertical lateral portion, both very thin and both separated by a right angle. The dorsal surface is slightly concave anteriorly, flattens in the midsection and then becomes convex posteriorly on the posterodorsal surface of the ventrally descending strut. In medial view (Fig. 3J), the postorbital shows the lateral wall and the distinct dorsal flange,

which contacts the supratemporal and squamosal laterally.

Supratemporal. The triradiate supratemporal (Figs 1A, C, D, E, 4) forms the posterolateral portion of the skull roof. It has three processes: anterolateral and anteromedial, which form the posterior half of the supratemporal fenestrae, and a thin sheet-like ventral process. In dorsal view (Fig. 4A), the two dorsal processes are similar in size and they form the posterior and lateral margins of the supratemporal fenestra. The rest of the dorsal surface is smooth, expands laterally and medially, and then narrows to a point at the end of the ventral process. Ventrally (Fig. 4B), the supratemporal is divided into medial and lateral sections. The medial section has a rugose surface, and a dorsoventrally orientated medial wall and shallow posterior concave bowl, both of which are smooth. The ventrolateral edge (Fig. 1E) slopes ventromedially until it reaches the concave bowl, where it descends ventrally. The medial edge is simpler, consisting of a ventrolateral concavity, which slopes to the tip of the ventral process. Laterally (Fig. 4E), the posterior bowl on the posteroventral surface is thin, and behind is a slim concave surface, and medially, the medialmost edge extends posteriorly and curves around to join the posterodorsal surface. This surface has a small projecting shelf posteriorly that forms the facet for the opisthotic portion of the paroccipital process.

Squamosal. The squamosal (Figs 1A, C, 5G–I) is a thin triangular element, with a thickened ventromedial edge that marks the facet for the quadratojugal. The anterior and lateral edges, where it overlaps the postorbital, are approximately straight. Laterally (Fig. 5I), the squamosal is thin and concave, while medially (Fig. 5H), the anterior half of the medial edge is thick and smooth, and slightly concave, forming the quadratojugal facet.

Quadratojugal. The small and thin quadratojugal (Figs 1A, C, 5C, D) is triangular, with the lateral surface formed from three planes: lateral, posterolateral and anterolateral. The lateral surface (Fig. 5C) is triangular and forms the posterior portion and margin of the lateral side, with the top point extending into a narrow medial ridge, which extends to the dorsalmost point of the lateral side. The postero- and anterolateral surfaces slope posteriorly and anteromedially, respectively. Medially (Fig. 5D), there is a smooth concavity, with a ventral lip. The quadratojugal contacts the supratemporal and squamosal anterodorsally, the quadrate posteriorly, the jugal anteriorly, and the postorbital both posteriorly and laterally.

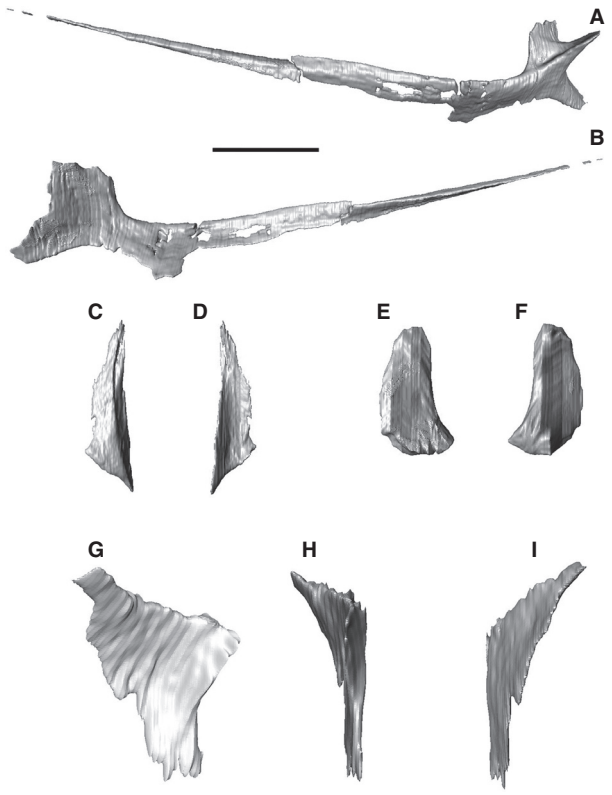

FIG. 5. Elements forming the posterolateral portion of the skull in BRLSI M1399. A–B, right pterygoid in medial (A) and lateral (B) views. C–D, right quadratojugal in lateral (C) and medial (D) views. E–F, right quadrate in lateral (E) and medial (F) views. G–I, right squamosal in anterior (G), medial (H) and lateral (I) views. Scale bar represents 20 mm.

Quadrate and palate

Quadrate. The quadrate (Figs 1A, C, 5E, F) is a stout and robust element that forms close associations with the stapes, pterygoid and quadratojugal. Viewed anterolaterally (Fig. 5E), the outline of the quadrate is reniform, widest ventrally. In posterior view, the quadrate widens ventrally, where it has a roughened surface, and both lateral and medial surfaces are concave. The medial surface (Fig. 5F) is smooth and concave, where the pterygoid is fused over a large area. Viewed ventrally, the quadrate condyle had a teardrop-shaped outline, rounded and bulbous posteriorly, and rounded anteriorly.

Vomer. The thin, elongate vomers (Fig. 6D–F) are poorly preserved, but appear to be almost complete, a rare occurrence in ichthyosaurs. Both vomers are present, yet only the right element is in correct position, as the left element, with the rest of the left side of the rostrum, is slightly twisted. Viewed along the anteroposterior axis, the vomer is nearly triradiate, formed from three plates:

dorsal, lateral and ventromedial. The dorsal portion increases in height from the posteriormost point and then steadily falls to an extremely narrow and needle-like anteriormost portion, which inserts between the premaxillae. This dorsal portion is also concave downwards in the posterior portion and loses this concavity anteriorly. The lateral plate is the smallest, and it curves slightly laterally, being widest in midsection, where it contacts the palatine. The ventromedial portion contacts the pterygoids, albeit restricted to a small section posteromedially.

Palatine. The medial section of palate is formed by the palatine (Fig. 6A–C), which lies between the jugal, maxilla and vomer. The palatine is a thin, laterally constricted element that thickens ventrally. The anteriormost portion is bifurcated into dorsal and ventral prongs, the first of which extends further anteriorly. The anterior end of the ventral surface shows a deep concave impression close to the bifurcations (Fig. 6C), which is also apparent on the dorsal surface, yet is much less prominent (Fig. 6A). On this dorsal surface, a shelf extends medially and becomes less prominent posteriorly, meaning the posterior third of the dorsal surface is smooth and laterally constricted (Fig. 6A). In the right side of the palate of BRLSI M1399, the palatine appears to be close to life position, and the dorsal bifurcation meets the posteromedial portion of the maxilla.

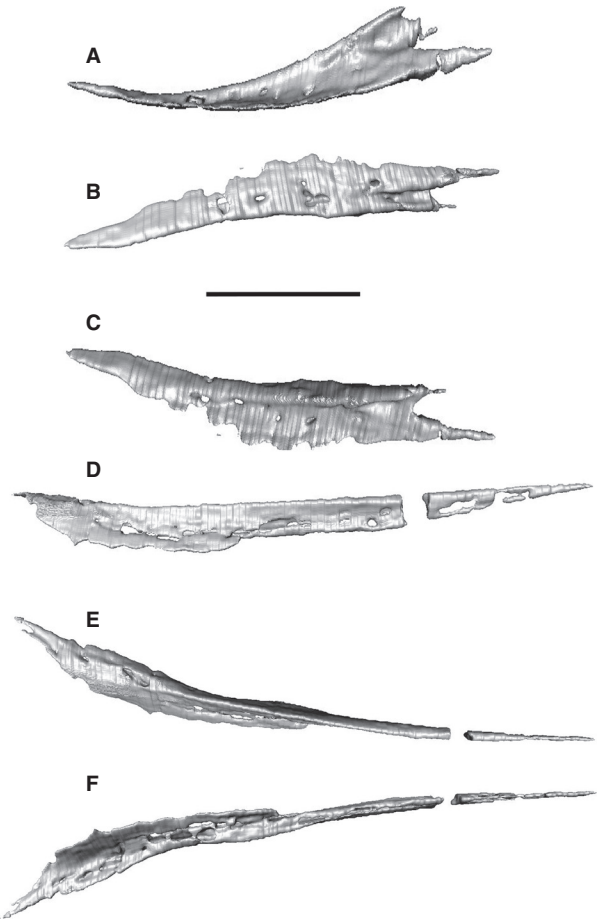

FIG. 6. Elements of palate of BRLSI M1399. A–C, right palatine in dorsal (A), medial (B) and lateral (C) views. D–F, right vomer in dorsal (D), medial (E) and lateral (F) views. Scale bar represents 20 mm.

Pterygoid. The pterygoids (Fig. 5A, B) are long, thin bones that are the largest elements in the palate. The posterior portion, the quadrate ramus, is complex, formed of three winged processes, dorsal, lateral and ventromedial, the last being the most robust, and the dorsal the largest and thinnest of the three. The dorsal and lateral processes converge anteriorly, making an acute angle, and where they meet, the pterygoid is at its thinnest, and the anterior ramus remains thin. The anterior ramus is laterally compressed and curved and becomes straight when viewed dorsally. The ventral edge faces medially in the posterior portion and then ventrally at the anterior end.

Mandible

Dentary. The dentary (Figs 1A–D, 7A, B), forming half the length of the jaw, is a long and straight element, with an almost straight ventral edge, and a slightly convex dorsal edge; it narrows posteriorly and anteriorly. The deep alveolar groove is positioned more laterally than in the premaxilla, and the second groove on the lateral surface is much more pronounced and extends from the anteriormost tip to where the alveolar groove stops (Fig. 7A). Medially (Fig. 7B), the surface is concave in the posterior portion, and the element becomes close to vertical anteriorly.

Splenial. The splenial (Figs 1B, D, 7B, D) covers the majority of the internal surface of the mandible. The medial surface is smooth and convex, and when viewed medially (Fig. 7D), the anterior end bifurcates into a dorsal and ventral extension, the latter of which is longer. The lateral surface is concave, and this curvature increases anteriorly, forming a pronounced longitudinal groove. This groove is the floor of the Meckelian canal, particularly clear in medial view (Fig. 7D).

Angular. The angular (Figs 1B, D, 7E, F) is slightly curved when viewed laterally (Fig. 7E), and the anterior end is narrower than the posterior end. The angular is concave in section, forming the floor of the Meckelian canal for two-thirds of the length of the mandible, and on its posterolateral margin to receive the posterior portion of the

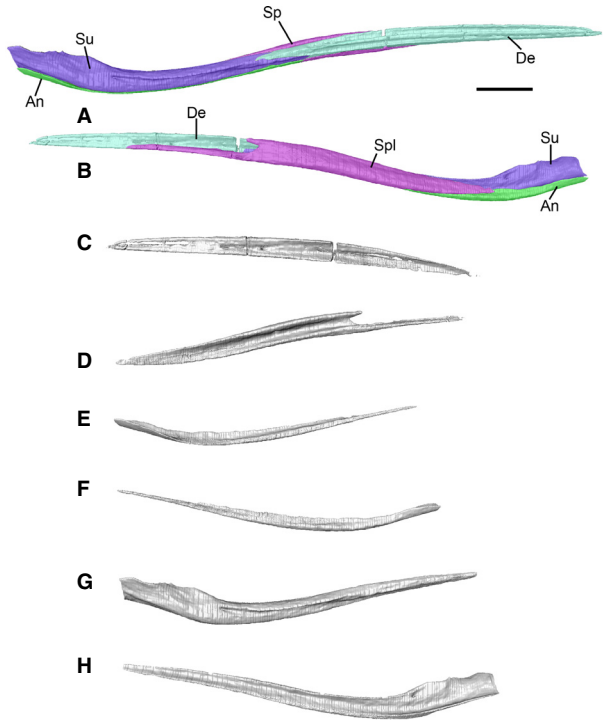

FIG. 7. Right mandible and mandibular elements of BRLSI M1399. A–B, right lower jaw in lateral (A) and medial (B) views. C, right dentary in medial view. D, right splenial in medial view. E–F, right angular in lateral (E) and medial (F) views. G–H, right surangular in lateral (G) and medial (H) views. *Abbreviations*: An, angular; De, dentary; Spl, splenial; Su, surangular. Scale bar represents 20 mm. Colour online.

surangular, and it loses this concavity as the element narrows to a point anteriorly. Medially (Fig. 7F), the surface is almost vertical and the ventral surface is rounded throughout.

Surangular. The surangular (Figs 1C, 7G, H) is a long, slightly curved element that narrows anteriorly. The lateral surface (Fig. 7G) is roughened and convex. Approximately one-third of the way from the posterior end is a narrow, pronounced longitudinal groove, the ventral lip of which disappears rapidly, but the dorsal lip becomes more pronounced and forms a ridge that extends longitudinally through the medial third of the surangular. Viewed laterally (Fig. 7G), the surangular terminates in a thin rounded edge anteriorly and a thick, almost straight edge posteriorly, and a shallow and elongate double-peaked process (paracoronoid process anteriorly and lower MAME process posteriorly; Fischer *et al.* 2012) is seen on the posterior section of the dorsal edge. Medially (Fig. 7H), the surface is smooth and concave, forming a wide and shallow groove for the lateral half of the Meckelian canal. The posterior end of the medial surface flattens as the dorsal edge slopes dorsally.

Prearticular. The narrow and laterally constricted prearticular (Fig. 8G–J) tapers at both ends, away from a centrally placed vertical portion. Posteriorly, the element terminates in a rounded edge, while the anterior end is narrow and pointed. The concave anterodorsal surface curves in such a way that it follows the curvature of the posterior dorsal edge precisely, and is hidden in lateral view (Fig. 8G). The posterior third of the element is in contact with the dorsomedial edge of the angular.

Dentition

In total, BRLSI M1399 has 150 teeth (Fig. 1A, B): 76 on the right side (33 dentary, 13 maxillary and 30 premaxillary) and 74 on the left side (29 dentary, 12 maxillary and 33 premaxillary). The teeth appear to be able to functionally interlock, and insert into a common dental groove in an aulacodont fashion, and no longitudinal ridges are apparent. The largest teeth in the specimen are towards the posterior portion of the mouth. The poor preservation in the dentition means little else can be described.

Hyoid apparatus

The hyoid apparatus (Figs 1D, 8A–F) is infrequently preserved in ichthyosaurs (Sollas 1916; McGowan and Motani 2003; Nicholls and Manabe 2004; Sander *et al.* 2011). In BRLSI M1399, the hyoid rod (ceratobranchial I; Motani *et al.* 2013) appears to be in life position on the right side of the skull. Each hyoid is tubular and hollow (Fig 8E, F), a feature never seen before in ichthyosaurs. The cross section of the hyoid bar changes along its length, being circular (Fig. 8F) posteriorly, and then laterally constricted towards the anterior end, giving the cross section an oval shape (Fig. 8E). This means that when viewed laterally, the height of the hyoid bar increases anteriorly. The hyoid bar begins to slope dorsolaterally towards the anterior end, so its lateral and medial surfaces are straight at the anterior end and convex at the posterior end. The hyoid bar contacts the flattened posteriormost section of the surangular and is aligned in such a way that the ventral margin of the angular and hyoid bar run almost parallel with one another. The bar also contacts the medial section of the prearticular.

Braincase

Variation in the structure of the braincase of post-Triassic ichthyosaurs is regarded as limited and conserved (Maisch and Matzke 2006) and is usually typified by the Liassic

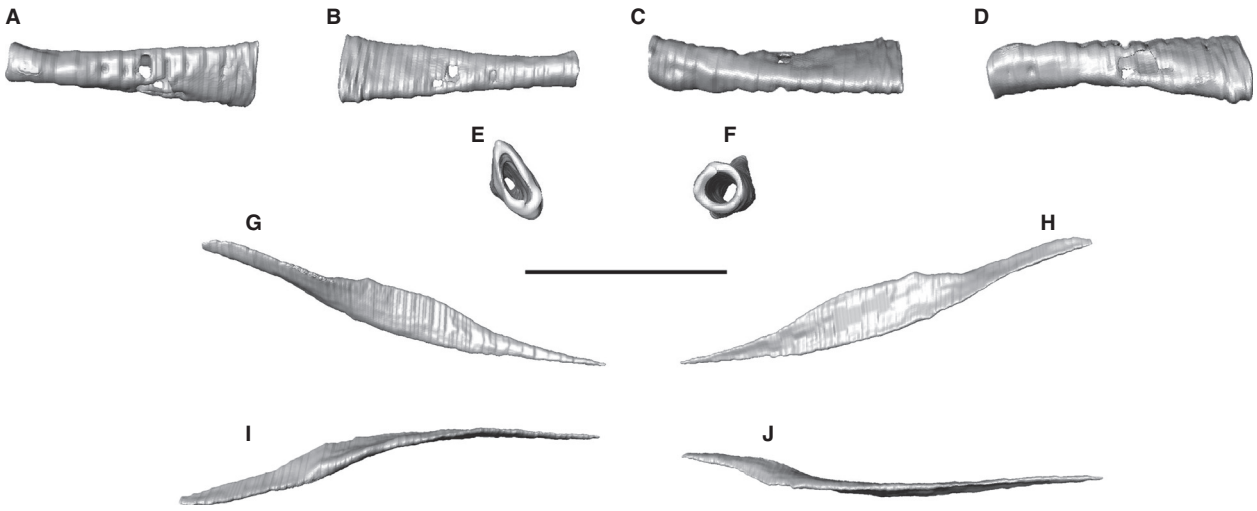

FIG. 8. Hyoid apparatus of BRLSI M1399. A–F, right ceratobranchial I in medial (A), lateral (B), anterior (C), posterior (D), anterior (E) and posterior (F) views. G–J, left prearticular in lateral (G), medial (H), dorsal (I) and ventral (J) views. Scale bar represents 20 mm.

Ichthyosaurus sp. (McGowan 1973). Our specimen largely agrees with previous descriptions. When reconstructed, the braincase of BRLSI M1399 is not strongly sutured, and only the basisphenoid and parasphenoid are fused.

Basioccipital. The basioccipital (Figs 9A, B, 10) is a robust, and somewhat rounded element, with a posteriorly protruding occipital condyle surrounded by the large, anteriorly sloping extracondylar area (Fig. 9A, 10A, B). The extracondylar area in BRLSI M1399 is not as large as in *Temnodontosaurus* or *Ichthyosaurus* (Owen 1881; McGowan 1973; McGowan and Motani 2003; Maisch 2002; Bennett *et al.* 2012), where it may equal or exceed the height of the basioccipital condyle. However, it is not as reduced as in the ophthalmosaurids *Ophthalmosaurus, Leninia* and *Arthropterygius chrisorum* (Andrews 1910; Kirton 1983; Maxwell 2010; Fischer *et al.* 2014) and is almost entirely lost in *Platypterygius* and *Brachypterygius* (Kirton 1983; Kear 2005). The dorsal margin of the basioccipital is slightly concave in the floor of the foramen magnum. Dorsally (Fig. 9A), the surface is rugose, with two rounded depressions, the exoccipital facets, placed either side of the midline. The anteriorly placed basioccipital peg is distinct and large, and especially prominent in lateral view (Fig. 10B). The tip of this is concave, similar to that of *I.* cf. *communis* described by McGowan (1973), although here that may be a result of breakage (Fig. 9A). A basioccipital peg seems to be limited to parvipelvian ichthyosaurs, particularly from the Lower Jurassic (McGowan and Motani 2003), and is not found in the few Triassic ichthyosaur braincases known (Merriam 1908; Maisch and Matzke 1997; Maisch *et al.* 2006; Maisch and Matzke 2006), or in the later ophthalmosaurids (Kirton 1983; McGowan and Motani 2003; Kear 2005). However, Kirton (1983) noted a small process in a specimen of *Ophthalmosaurus icenicus* (GLAHM V1070) that was interpreted as the homologue of the basioccipital peg. Anteriorly and immediately to the right of the basioccipital peg is a deep triangular depression (Fig 9B), which extends posterolaterally, terminating at a point around the lateral midline. McGowan (1973) described a similar, but more laterally positioned feature in *Ichthyosaurus*, and attributed this to marking the position of the lagena. The left lateral surface is smooth, while the right side is much more rugose.

Supraoccipital. The supraoccipital (Figs 9C, D, 10) forms a high, curved arch, roofing the foramen magnum, and forming only a small part of its height, as it does in *Ichthyosaurus* and *Temnodontosaurus* (Owen 1881; McGowan 1973; Maisch 2002). The contribution of the supratemporal to the foramen magnum is much larger in the ophthalmosaurids *Ophthalmosaurus* and *Platypterygius* (Andrews 1910; Kirton 1983; Kear 2005), where it may form most of its height. The posterior surface faces anteroposteriorly and is smooth, and convex, becoming flatter towards the exoccipital facets. Laterally, this is pierced by one foramen on each side that continues through to the medial face of the supratemporal (Fig. 10D). On the right side, there are two indentations; the more ventral of these is deeper. The triangular, concave exoccipital facets occupy the entire ventral surface, tapering to a point anteriorly. The long axes of these facets are aligned parallel, not divergent as in *Ichthyosaurus* or *Temnodontosaurus*, but more similar to *Ophthalmosaurus* (McGowan 1973; Kirton 1983; Maisch 2002). Laterally (Fig. 10B),

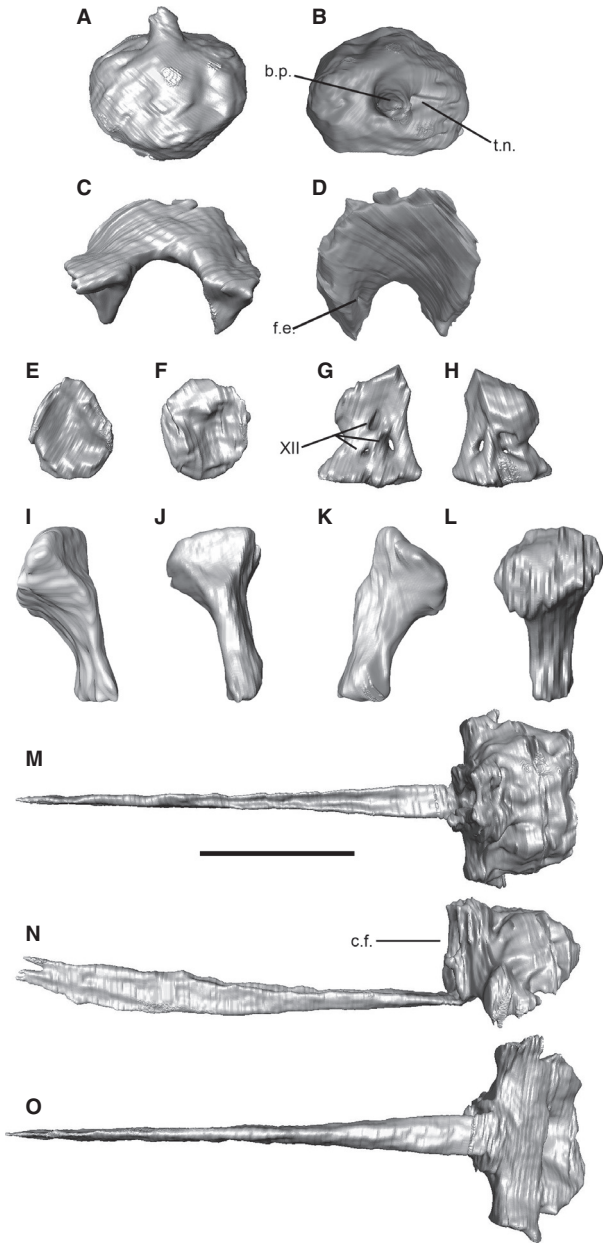

FIG. 9. Braincase components of BRLSI M1399. A–B, basioccipital in dorsal (A) and posterior (B) views. C–D, supraoccipital in posterior (C) and anterior (D) views. E, right prootic in posterior view. F, right opisthotic in anterior view. G–H, right exoccipital in lateral (G) and medial (H) views. I–L, right stapes in posterior (I), lateral (J), anterior (K) and medial (L) views. M–O, parabasisphenoid in dorsal (M), lateral (N) and ventral (O) views. *Abbreviations*: b.p., basioccipital peg; c.f., carotid foramen; f.e., foramen endolymphaticum; t.n., triangular notch; XII, branches of the hypoglossal (XII) nerve. Scale bar represents 20 mm.

there are two large grooves, the posteriormost of which begins at the posteroventrally flattened shelf of the posterior surface and ends in a ridge at the dorsoventral midline. Both grooves extend dorsoventrally for the entire length of the flattened shelf, but the anteriormost continues further forwards, as seen in both lateral and anterior views (Fig. 10B, C). On the right side of the ventral anterior surface (Fig. 10C), towards the facets, lies a single deep notch, similar to those on the posterior surface.

The deeper of the two anterior foramina in the supraoccipital of BRLSI M1399 is near where McGowan (1973) and Maisch (2002) placed the foramen endolymphaticum (Fig. 9D), which houses the endolymphatic ducts in extant squamates; the anterior foramen in BRLSI M1399 may have served a similar purpose. Alternatively, these foramina may be exit points for the occipital vein (Kirton 1983). Regardless of their function, the distribution and number of these foramina is different from other taxa. While similar to those of *Temnodontosaurus* and *Ichthyosaurus* (McGowan 1973; Maisch 2002), these taxa show mirrored foramina, as do Cretaceous taxa, such as *Athabascasaurus bitumineus* and *Platypterygius australis* (Kear 2005; Druckenmiller and Maxwell 2010). The asymmetrical foramen arrangement seems unique to BRLSI M1399.

Prootics. Both prootics (Figs 9E, 10B–D) are present, with the left prootic being harder to discern in cross section, owing to poor scan quality in this area. These elements are slender, wider ventrally and medially. The anterior surface is convex and roughened, with a low ridge along the dorsoventral midline that may be the attachment point of the M. adductor mandibulae externus (Kirton 1983; Kear 2005). Laterally, the element becomes lower, with a dorsolaterally facing concave shelf positioned dorsally. Posteriorly, there is a V-shaped groove (Fig. 9E), dorsally placed and smoother than the surrounding bone, which marks the paths of the semicircular canals (McGowan 1973; Kirton 1983). Depending on the preservation and the ossification, these impressions may be extended and appear more T-shaped (McGowan 1973; Kear 2005; Fischer *et al.* 2011). They are less prominent in BRLSI M1399, giving the impression a pear-like appearance, suggesting that here the prootics only contact the anteriormost point of the semicircular canals. The margin of the prootic is grooved and roughened where the surrounding cartilage would have held it. The prootic in *Sveltonectes insolitus* is pierced centrally by a foramen (Fischer *et al.* 2011), but the phylogenetic significance of this within Parvipelvia is unclear as it is only shared in Triassic taxa.

Opisthotic. The opisthotic (Figs 9F, 10) is a relatively small, robust element, unlike those of non-parvipelvians such as *Phantomosaurus neubigi* and *Mixosaurus cornalianus* (Maisch and Matzke 2006; Maisch *et al.* 2006), in which the paroccipital process is unusually long and anteroposteriorly narrow, forming a plate-like shape. The posterior surface is concave in lateral view and convex,

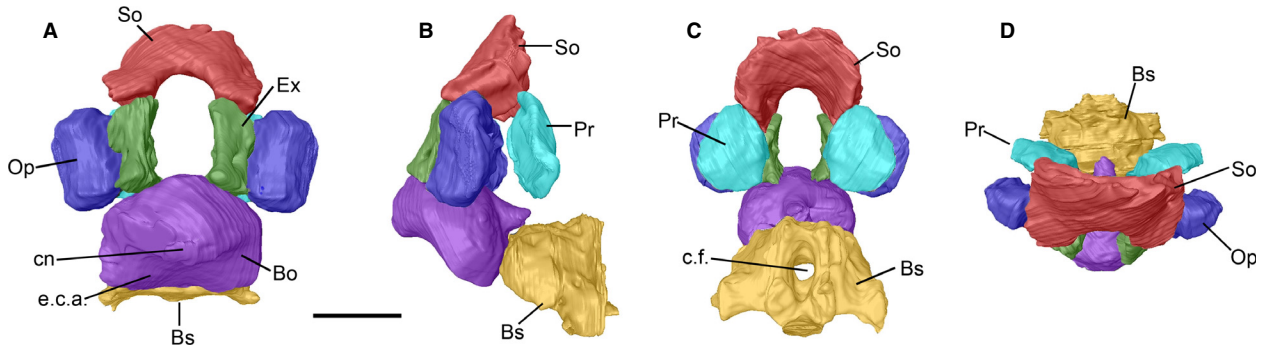

FIG. 10. Reconstructed braincase of BRLSI M1399 in posterior (A), lateral (B), anterior (C) and dorsal (D) views. *Abbreviations*: Bo, basioccipital; Bs, basisphenoid; c.f., carotid foramen; cn, condyle; e.c.a., extracondylar area; Ex, exoccipital; Op, opisthotic; Pr, prootic; So, supraoccipital. Scale bar represents 20 mm. Colour online.

almost triangular dorsoventrally, and a medial ridge extends dorsoventrally, while the anterior surface appears concave. The dorsal and ventral surfaces terminate in a rounded point, and the thickness of the element seems to increase medially. Dorsally, the left opisthotic appears triangular with a concave anterior surface that bears four ridges, around two concavities, and a single median peak. The median peak sits on the lateral midline and between the concavities, and above it lies the triangular and robust paroccipital process. This process descends posterodorsally, and in lateral view (Fig. 10B), it is relatively thick. In right lateral view (Fig. 10B), there is a ridge that extends to the ventralmost point of the lateral concavity, possibly part of the channel housing either the glossopharyngeal (IX) nerve or the main hyomandibular branch of the facialis (VII) nerve, as in *Platypterygius australis* (Kear 2005, p. 606) and *Ophthalmosaurus* (Appleby 1961, p. 338). In lateral view (Fig. 10B), the opisthotic reaches its widest point medially and tapers dorsoventrally.

In neoichthyosaurians, opisthotic morphology is reasonably similar throughout, although the form of the paroccipital process allows for differentiation of species. In this regard, the opisthotics of BRLSI M1399 are most similar to those of *Ichthyosaurus communis* and *Ophthalmosaurus icenicus* (McGowan 1973; McGowan and Motani 2003), although the paroccipital process is more pronounced and exteriorly offset in these taxa. *Hauffiopteryx* appears to be the only neoichthyosaurian in which the paroccipital process is so distinct (Maisch 2008; Caine and Benton 2011). The opisthotics of platypterygiines are more dorsoventrally constricted, as in *Pl. australis* (Kear 2005), which agrees with the phylogenetic placement of *H. typicus* (Fischer *et al.* 2013). Some novel features can be found on the anterior face of the opisthotic of BRLSI M1399 and its associated impressions on the otic capsule. Previous reconstructions have made the posterior semicircular canal ventrally downturned, yet in BRLSI M1399, it appears somewhat straightened, shorter and wider.

Exoccipitals. The exoccipitals (Figs 9G, H, 10) are small, robust, with broad dorsal and ventral ends, expanded anteroposteriorly. Three foramina pass mediolaterally through the middle portion (Fig. 9G) and are interpreted as the paths of branches of the hypoglossal (XII) nerve (Kirton 1983). This is more than in *Sveltonectes insolitus* (one), *Athabascasaurus bitumineus* (two) and most specimens of *Ophthalmosaurus icenicus* (two) (Andrews 1910; Kirton 1983; Maisch 1997; Druckenmiller and Maxwell 2010; Fischer *et al.* 2011), but both *Ichthyosaurus* and *Temnodontosaurus* have three foramina (McGowan 1973; Maisch 2002), while *Platypterygius australis* may have more (Kear 2005). These foramina are all of similar, but the anteriormost foramen is smallest, and together, they form a triangle, a unique feature among Ichthyopterygia; in other taxa, they are arranged in a line (Maisch 2002; Kear 2005; Maisch and Matzke 2006). In lateral view (Fig. 9E), the anteriormost two foramina appear to lie in the same depression, separated by a ridge from the posterior foramen. The three foramina are also seen clearly in medial view (Fig. 9G), with the anterior separated by a ridge from the two posterior foramina. The variation in these foramina, and its bearing on phylogeny, are debated with some suggesting that variation between individuals of the same species is high (Maisch 1997): an individual of *Ophthalmosaurus icenicus* (SMNS 10170) possesses a total of five foramina, three in the right element and two in the left. Maisch (1997) concluded that foramen variability should be used with caution in phylogenetic analyses. The anterior surface is infolded at mid-height, and the posterior surface is more nearly vertical. The dorsal, rounded facet for contact with the supraoccipital is clear in lateral view (Fig. 9H), and the facet for contact with the basioccipital is entirely ventrally located, extended in a similar manner to other basal thunnosaurians, such as *Ichthyosaurus* and *Stenopterygius* (Owen 1881; McGowan 1973; Godefroit 1993, 1994).

Stapes. The stapes comprises an enlarged dorsomedial head and a more gracile, ventrolateral shaft (Fig. 9I–L).

The medial head is broad, convex and roughened for the application of cartilage, as this would be applied to facets on the basioccipital and basisphenoid. Laterally, the stapes narrows into a flattened bar directed towards the quadrate, which is contacted with a small, flattened facet. In posterior view (Fig. 9I), the dorsal third of the mediolateral surface is concave, most likely the opisthotic facet, while the ventral surface appears flat. Both the anterior and posterior surfaces are concave, with the former being mainly smooth, with a small rugosity in the dorsomedial section of this surface, while the posterior surface is more rugose.

Both *Ichthyosaurus* and *Ophthalmosaurus* have a similar form of the stapes as BRLSI M1399, with a broad medial head and more slender lateral bar (McGowan 1973; Kirton 1983). In *Ichthyosaurus* particularly, the medial facets may be well defined by a transverse groove that separates them and probably transmitted stapedial artery (McGowan 1973). However, in *Temnodontosaurus,* the stapes is much more robust, the shaft is poorly delimited, and the medial and lateral ends may be similar in size, as in *Temnodontosaurus azerguensis* (Maisch 2002; Martin *et al*. 2012). This contrasts with the more slender lateral stapes found in more derived ophthalmosaurids, such as *Janusaurus lundi* and *Mollesaurus periallus* (Fernández 1999; Roberts *et al.* 2014).

Parabasisphenoid. The parabasisphenoid (Fig. 9M–O) comprises the broad, robust basisphenoid (Fig. 10B, C), fused to the elongate, slender parasphenoid directed anteriorly. The front of the parasphenoidal portion is laterally compressed, narrowing and rising anteriorly, creating a slightly ventral curvature. Behind this, it is grooved dorsally (Fig. 9M), likely for reception of the trabecular cartilage (Kirton 1983), and becomes dorsoventrally flatter towards the basisphenoid. In lateral view (Fig. 9N), there are three small, dorsoventrally orientated peaks. The basisphenoidal portion is highly rugose texture on all surfaces except for the entire ventral surface, and the anterior and lateral surfaces of the wing-like basipterygoid processes. In lateral view (Fig. 9N), there are two deep notches ventrally on the basipterygoid processes, with one almost directly above the other. The single carotid foramen (Fig. 9N, 10C) pierces the basisphenoid medially on the anterior face, above the base of the parasphenoid, exiting in the posterior portion of the ventral surface (Fig. 9O). In *Temnodontosaurus*, the ventral exit of the carotid artery is paired (Maisch 2002; Martin *et al.* 2012). Above the anterior exit of the carotid foramen is a small ovoid cavity, the pituitary fossa, as identified also in *Ichthyosaurus* and *Ophthalmosaurus* (McGowan 1973; Kirton 1983). Around this, the anterior face rises to the dorsum sellae, a pair of pitted, flattened processes that face dorsally at the top of the basisphenoid (Fig. 9M, N). Just above the contact with the parasphenoid are two petaloid facets, both slightly concave, that likely mark the base of the trabecular cartilage (Kirton 1983). The basipterygoid processes are widest distally and narrow slightly at mid-length. In lateral view (Fig. 9N), the basipterygoid processes are triangular, with the point facing posteriorly. These are better developed and more distinct from the main body of the basisphenoid than in *Temnodontosaurus*, *Ichthyosaurus* and even the more derived ophthalmosaurids *Platypterygius australis* and *Sveltonectes insolitus* (McGowan 1973; Maisch 2002; Fischer *et al.* 2011); this is more similar to that of *O. icenicus* (Kirton 1983). We do not see evidence of vessel grooves behind the basipterygoid processes, as has been reported in *Ophthalmosaurus icenicus* and *Pl. australis* (Andrews 1910; Kirton 1983; Kear 2005), although this may be due to the subadult nature of the specimen.

Reconstructed braincase

The braincase was reconstructed (Fig. 10) based on the anatomy of the digital skull, and on previous reconstructions, primarily McGowan (1973) and Romer (1968). The basisphenoid and parasphenoid have been rotated along the dorsoventral axis, so that the parasphenoid is in line with the sutures of the parietals and frontals. A loose union now exists between the basioccipital and the basisphenoid, so that the basioccipital peg faces anteriorly and is aligned with the narrow central fissure on the posterior surface on the basisphenoid. Contact is now made between the ventral surface of the exoccipitals and the exoccipital facets on the basioccipital. Both exoccipitals have been rotated so that the foramina pass through mediolaterally. With the basioccipital and exoccipitals in place, the floor and lateral margins of the foramen magnum are reconstructed. The supraoccipital rests on top of the exoccipitals, but, as is true for all the other contacts between elements of the braincase, intervening cartilage would have precluded a direct contact (McGowan 1973; Kirton 1983). The supraoccipital is rotated so that the dorsalmost lateral grooves align with the interior margin of the supratemporal. This rotation also allows the dorsal flange to align with the parietals.

The opisthotics now lie between the supratemporal and the exoccipitals. They have been rotated so that the concave anterior surface faces inwards. Anteriorly, the prootics do not contact any other element because of cartilage. However, using Romer (1968, figs 6 and 9) as a comparison, a reasonable estimation was attained. The prootics are now in line with the anteriormost point of the dorsolateral groove of the supraoccipital. They have been rotated so that the concave surface now faces posteriorly, and the thicker of the two lateral ridges faces exteriorly, while the thinner, straighter edge, which forms the lateral

shelf, laterally bounds the border between the cerebellum and the optic lobes.

Endocast

It was possible also to reconstruct an almost complete cranial endocast, together with three hypoglossal nerves and an incomplete otic capsule (Fig. 11). Because the braincase is dominated by cartilage and muscles, the true ventral extent of the endocast could not be reconstructed. However, many features can be discerned, from front to back: olfactory lobes, cerebrum, pineal organ, optic lobes, cerebellum and medulla oblongata. Overall, the brain is curved, from the ventralmost tip of the cerebellum, in line with the basioccipital peg, and increasing anteriorly. The brain occupies approximately one-third of the length of the skull, extending from the exoccipitals to the internasal foramen.

The forebrain is represented by the partial olfactory lobes and the cerebrum. As the ventral extent of the forebrain is uncertain, only the dorsal telencephalic region can be documented, while the ventrally orientated diencephalic region, which includes the thalamus, epithalamus and the hypothalamus (Porter 1972), cannot be reconstructed. The telencephalon appears to comprise the anterior olfactory bulbs and the medial cerebral hemisphere and pineal organ. The ventral surfaces of the frontals bear impressions of the olfactory lobes. Despite only a partial reconstruction, the olfactory lobes still have a substantial anteroposterior extent, as large as, if not larger than, the optic lobes, the most prominent of the cephalic regions. The olfactory lobes are dorsoventrally narrow and rather shallow, but probably did not extend much further ventrally than displayed in Figure 11. The cerebral hemisphere extends further laterally than anteroposteriorly and bounds the medial pineal organ, which forms a pronounced peak, giving the cerebral hemisphere a triangular appearance in anterior view (Fig. 11C). The lateral sides of the cerebral hemisphere are strongly curved.

The reptilian brainstem comprises the mesencephalon and rhombencephalon (Schaeffer and Waters 1996), both of which are represented in the encephalic cast of BRLSI M1399. The optic lobes form the entirety of the mesencephalon, and they are framed as impressions on the ventral faces of the parietals and are clearly a major component of the brain, as they occupy the dorsoventrally thickest part. In line with the point, and on both external sides of the brain, there are two lateral, symmetrical bulges, which are lateral extensions of the optic lobes. These bulges can be seen best in dorsal and posterior views (Fig. 11C, D). In lateral view, the dorsal surfaces of the protuberances extend anteriorly, forming ridges that terminate at the border between the optic lobes and the cerebrum. In posterior view (Fig. 11C, D), the optic lobes

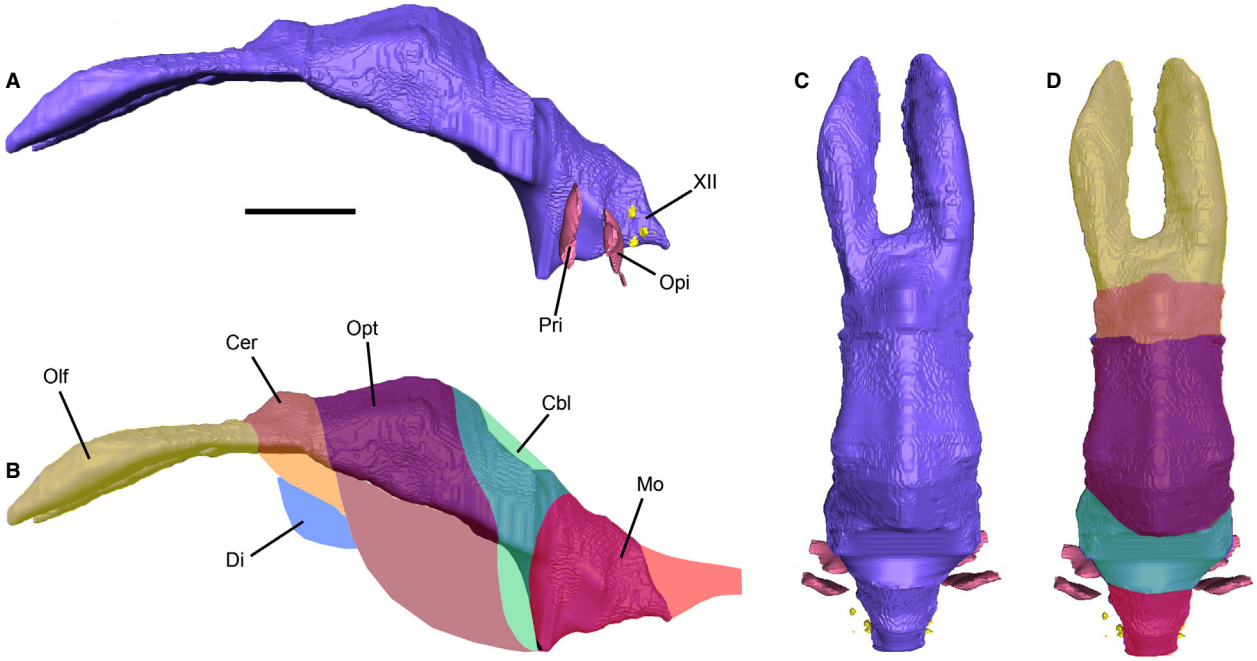

FIG. 11. Cranial endocast of BRLSI M1399. A, lateral view. B, lateral view, showing hypothesized sizes of neurological regions. C, dorsal view. D, dorsal view showing hypothesized size of neurological regions. *Abbreviations*: Cer, cerebral hemisphere; Cbl, cerebellum; Di, hypothesized proportions of the diencephalon; Mo, medulla oblongata; Olf, olfactory region; Opi, endosseous labyrinth impression from the opisthotic; Opt, optic lobe; Pri, endosseous labyrinth impression of the prootic; XII, branches of the hypoglossal (XII) nerve. Scale bar represents 20 mm. Colour online.

converge in a point, where the two parietals join, making a somewhat triangular overall shape. The rhombencephalon consists of the cerebellum and the medulla oblongata (Ten Donkelaar and Bangma 1979). The cerebellum forms an impression on the anterior surface of the supraoccipital, and it is laterally wide and increases in width anteriorly, towards the posterior border of the optic lobes. The dorsal surface of the cerebellum slopes posteroventrally. Because of the gap between the dorsal surfaces of the parietals and the supraoccipital, the true dorsal extent of the cerebellum could not be reconstructed. However, the dorsal curvature most likely steepened anteriorly. The medulla oblongata is thin and laterally constricted, and it formed impressions on the exoccipitals on either side. Ventrally, the surface can be reconstructed with reasonable accuracy, as it is framed by the dorsal surface of the basioccipital and the basioccipital peg. This surface slopes posterodorsally, and the dorsal surface slopes posteroventrally, making the medulla oblongata thinner posteriorly, and the ventral surface laterally thinner than the dorsal surface.

Other elements of the reconstructed endocranium are the cranial nerves and the otic capsule, both of which are incomplete and lie on either side of the rhombencephalon. Branches of the hypoglossal (XII) nerve passed through the three foramina in each of the exoccipitals. They are all thin and arranged in a triangular pattern on either side of the medulla oblongata, with one placed dorsally and two ventrally. On either side of the cerebellum lie the otic capsules, which made impressions on the opisthotics posteriorly, the prootics anteriorly and the supraoccipital interiorly. Their reconstructed extent is speculative, but the impressions of the opisthotics and prootics are almost identical to those presented in McGowan (1973, figs 39, 40). Impressions of the opisthotics are V-shaped, showing two channels meeting at a wide, rounded base. The posteriormost channel may have housed the posterior vertical semicircular canal, and the anteriormost channel may have housed the horizontal semicircular canal (Kirton 1983), while the wide rounded based may have housed part of the ampulla. Impressions of the prootic seem much simpler, being round, with a convex interior surface and a slightly concave exterior surface. These may have made contact with the sacculus, the utriculus, the ampulla (Andrews 1910; Kirton 1983; Kear 2005) and perhaps the vertical and horizontal semicircular canals. Owing to the lack of preserved cartilage, the endosseous labyrinths could not be constructed, as done by McGowan (1973, fig. 41).

Phylogenetic placement of BRLSI M1399 and H. typicus

The exact search in TNT recovered nine most parsimonious trees of length 147 steps. The consistency and retention indices for the strict consensus of these trees are 0.366 and 0.599, respectively, and the rescaled consistency index is 0.219. In total, 14 characters were modified for *Hauffiopteryx typicus* from Fischer *et al.* (2013) based on the exclusion of the BRLSI material (see Marek *et al.* 2015). Twenty-nine characters in BRLSI M1399 are coded differently from *H. typicus*: 16 skull and 13 postcranial characters, of which 16 are uncertain in *H. typicus*. The topology recovered in strict consensus (Fig. 12) is similar, but less well resolved than that of Fischer *et al.* (2013). We recover both BRLSI M1399 and *H. typicus* as more derived than *Ichthyosaurus communis*, and thus within Thunnosauria, but not monophyletic with each other. This placement of *H. typicus* is more similar to the phylogenies presented by Maisch (2008) and Maxwell *et al.* (2012). Most ophthalmosaurid taxa (excluding *Arthropterygius chrisorum*) form a large polytomy, caused by instability of many taxa included within this clade. Also, the relationship between *Hudsonelpidia brevirostris* and *Macgowania janiceps* is not resolved. Bremer support values are generally low (Marek *et al.* 2015, fig. S1), but Ophthalmosauridae receives a decay index of five, and the internal clade, excluding *Arthropterygius chrisorum*, has a decay index of 10. Resampling values are also low, mostly <50%, and there is infrequently support for clades with high Bremer support, but again, the clade within Ophthalmosauridae receives a comparatively higher support of 69%. Resampling supports are mostly higher here than in Fischer *et al.* (2013), but only moderately. This may reflect the different method used (symmetrical vs bootstrap and jackknife resampling): similar differences were found on a rerun of the original data with symmetrical resampling.

DISCUSSION

Comparative remarks

The relative completeness of BRLSI M1399 allows further insight into the phylogenetic affinities of the genus *Hauffiopteryx*. This taxon had previously been positioned outside Thunnosauria by Fischer *et al.* (2013), as its immediate sister group. Maxwell *et al.* (2012) found a poorly resolved basal Parvipelvia, but *H. typicus* was again found to be more derived than *Ichthyosaurus communis*, and close to *Leptonectes tenuirostris*. Maxwell *et al.*'s (2012) and our relationships broadly match those hypothesized by Maisch (2008), despite his phylogenetic argument that did not use cladistic methods. Maisch (2008) identified the German *H. typicus* as a basal stenopterygiid, but with some resemblances to leptonectids, partially confirmed by Caine and Benton (2011), who did not identify a monophyletic Stenopterygiidae, and placed

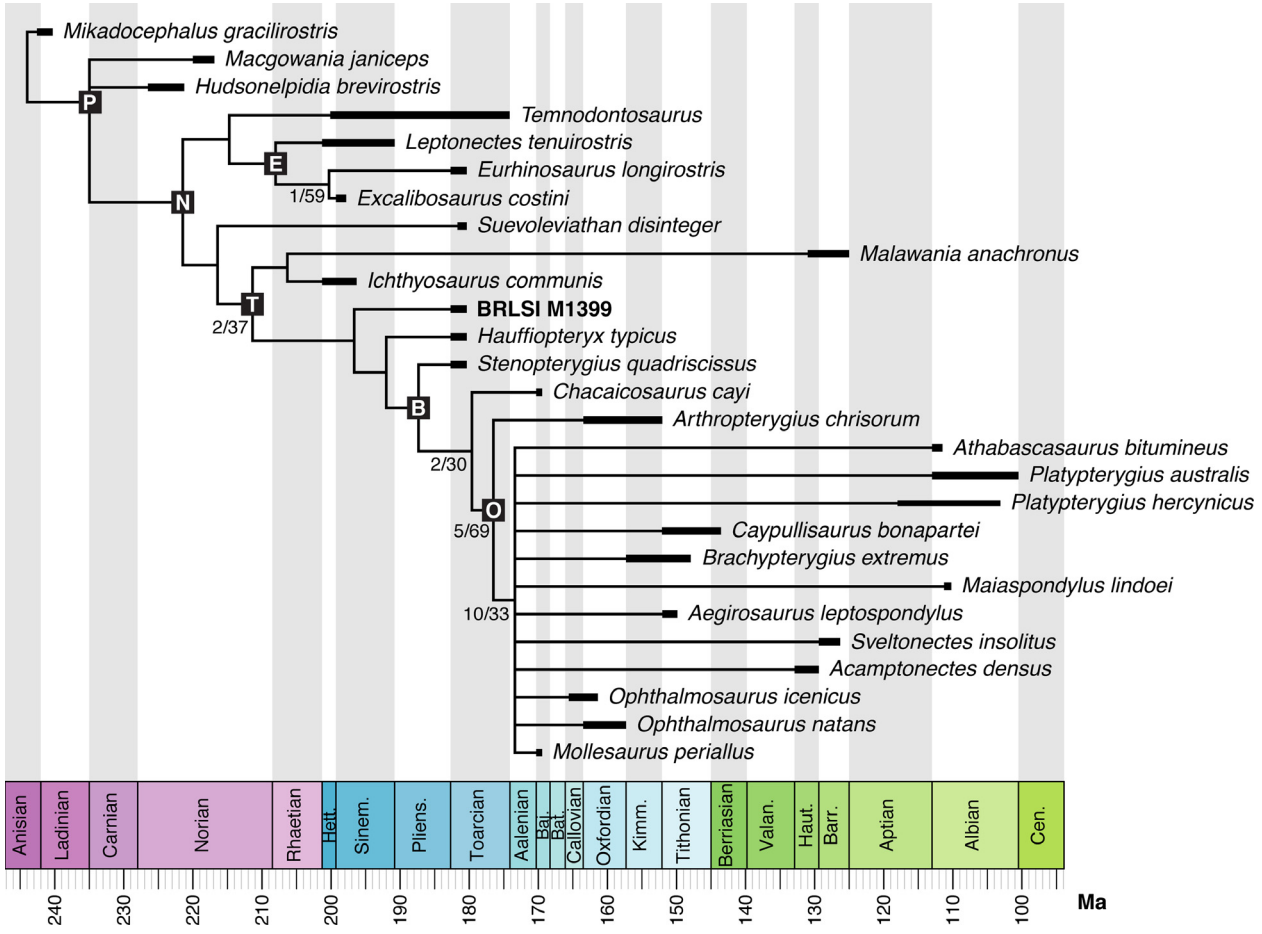

FIG. 12. Time-calibrated strict consensus of nine most parsimonious trees resulting from exact analysis in TNT, with BRLSI M1399 coded as a new terminal taxon in the modified matrix of Fischer *et al.* (2013). Calibration of nodes used the equal-age method of Brusatte *et al.* (2008). Clade supports are indicated where Bremer support >1 or symmetrical resampling >50%. See Marek *et al.* (2015) for methods and occurrence data. B, Baracromia; E, Eurhinosauria; N, Neoichthyosauria; O, Ophthalmosauridae; P, Parvipelvia; T, Thunnosauria. Colour online.

Hauffiopteryx, including the Bath specimens, either close to Thunnosauria or Eurhinosauria. The thunnosaurian synapomorphies in *H. typicus* (Maisch 2008) weaken the argument for a close relationship between *Hauffiopteryx* and Leptonectidae. There are many resemblances between BRLSI M1399 and *H. typicus* (Caine and Benton 2011), and these taxa are placed phylogenetically as a transitional group between basal and more derived neoichthyosaurians and thunnosaurians, such as the ophthalmosaurids (Fischer *et al.* 2013). These taxa are not monophyletic, however, and there are many character differences between BRLSI M1399 and the Belgo-German *H. typicus* material (Marek *et al.* 2015). There may be cause to revise this material based upon the new insights afforded by additional preparation and new visualisation techniques.

BRLSI M1399 shows many external features regarded as diagnostic for leptonectids (Maisch 1998, 1999; McGowan and Milner 1999; Maisch and Matzke 2000, 2003): large orbit, small supratemporal fenestrae, a shortened postorbital skull segment, slender and elongated conical teeth that lack distinct surface ornamentation of the enamel, as well as a long and delicate snout. Ecological convergence may be at play here, as seen between *Temnodontosaurus azerguensis* and *Leptonectes* (Martin *et al.* 2012). The previously unresolved characters of BRLSI M1399, and those that are now seen as different from *H. typicus*, are found almost exclusively in more advanced members of Thunnosauria, such as the ophthalmosaurs: absence/subtle root striations, absence of the processus narialis of the maxillae, presence of the processus temporalis of the frontal, wing-like basipterygoid processes, absence of ventral notch of extracondylar area of basioccipital, and ischium/ischiopubis is rod-like rather than plate-like. These all cast doubt on the former assignment of BRLSI M1399 to *Hauffiopteryx*.

Some of the anatomical features of the skull in BRLSI M1399 are unusual, exceptionally rare, or have never been

previously documented in ichthyosaur descriptions. The remarkable preservation of the right side of the skull has preserved elements such as the vomer, palate, prearticular and the hyoid bar in detail, and close to where previous authors have postulated they would have been in life (Romer 1968; McGowan 1973). Perhaps the best example is the hyoid apparatus, which is rarely documented in ichthyosaurs (McGowan 1973; Kear 2005; Kolb and Sander 2009; Fischer *et al.* 2011; Sander *et al.* 2011). In BRLSI M1399, not only is it preserved both in three dimensions and close to life position, but also the fact that the hyoid bar is hollow has not been documented before. The function of this feature is unclear and may reflect the juvenile status of BRLSI M1399. The prearticular is also preserved and confirms previous ideas of its true placement.

Endocast and sensory biology

Digital endocasts only provide evidence of the gross morphology of an extinct organism's neuroanatomy (Hopson 1979; Rogers 2005). This is unfortunate, as internal brain structures can aid in identification of certain amniote groups, such as the diapsid-specific dorsoventricular ridge (DVR) in the telencephalic region (Nomura *et al.* 2013). However, in BRLSI M1399, the external morphology of the endocast was probably similar to the gross neuroanatomy of many extant neodiapsids, including lepidosaurs, crocodilian archosaurs and chelonians (Ten Donkelaar and Bangma 1979), and so cannot test hypotheses of the placement of Ichthyopterygia in amniote phylogeny.

As ichthyosaurs had the largest relative and absolute eyeball size of any vertebrate (Motani *et al.* 1999), it is unsurprising that the optic lobes are among the most prominent features in the endocast of BRLSI M1399, confirming the primacy of vision. It should be noted that correlations between eye size and brain size have been documented in birds (Burton 2008; Iwaniuk *et al.* 2008) and primates (Barton 2004). This may also be true for ichthyosaurs, but as yet there are not enough available measurements of ichthyosaur brain size to test this hypothesis. Compared to the standard reptilian model (Porter 1972), the cerebellum is enlarged. This is also true in highly derived aquatic vertebrates such as cetaceans (Slijper 1962; Webb and de Buffrénil 1990) and suggests that ichthyosaurs had a high degree of locomotory ability and coordination, as suggested previously (McGowan 1973; Kirton 1983). The cerebral hemispheres are also somewhat enlarged, suggesting that ichthyosaurs relied on innate, instinctive behaviour, with little capacity for learning; Quay (1979) and Kirton (1983) noted the possibility that cerebral hemispheres in other reptiles could be enlarged beyond the parietal foramen. These observations corroborate previous assumptions on ichthyosaur sensory biology and neuroanatomy, made from latex casts (McGowan 1973) and endocephalic impressions of the ventral surface of the skull roof (Maisch 1997).

Some features of the endocast of BRLSI M1399 are new. Previous interpretations of the ichthyosaurian brain posited that the olfactory region is somewhat reduced (Maisch 1997), but in BRLSI M1399, the olfactory region (olfactory bulbs and olfactory tracts) is enlarged. While unexpected, McGowan (1973) and Kirton (1983) both hypothesized that, with no secondary palate, the nasal canals in ichthyosaurs were in direct contact with the buccal cavity, rather than the lungs. Thus, the external nares did not have to be closed when the animal was submerged, as in crocodilians and cetaceans. This would have allowed ichthyosaurs to employ their olfactory system when underwater, for reproductive function and detecting conspecifics, or indeed predators, via exhaled breaths or to track prey, as hypothesized for other aquatic vertebrates with a relatively enhanced sense of olfaction, such as baleen whales (Thewissen *et al.* 2010).

In comparison with the endocasts of other marine reptiles, BRLSI M1399 had an elongate brain, as in nothosaurs and plesiosaurs, but not so short as in placodonts (Neenan and Scheyer 2012). The shortening of the placodont skull and brain gives it a sharper upward bend between the medulla oblongata and cerebellum, as well as overall shorter and broader cerebellum. Sensory regions of this placodont endocast could not be distinguished, partly because the anterior portions of the braincase wall are not ossified. A reconstructed metriorhynchid crocodilian endocast (Fernández *et al.* 2011) also lacks the forebrain and does not provide clear insights into sensory regions. The brain overall is elongate, as in BRLSI M1399, corresponding to the elongate skull in ichthyosaurs and metriorhynchids. Natural casts of the anterior endocast in the snout of metriorhynchids (Herrera *et al.* 2013; Herrera and Vennari 2015) show reduced olfactory bulbs and olfactory nasal region, suggesting that these marine Jurassic crocodilians lacked the aerial olfactory sense of modern crocodiles.

CONCLUSIONS

Computed tomographic scanning of an exceptional specimen of a Toarcian ichthyosaur has furthered the knowledge of the cranial anatomy and phylogeny of ichthyosaurs, revealing some unusual structures such as the tubular hyoids. The scans have permitted the first digital reconstruction of an ichthyosaur endocast, and this has provided data to infer aspects of the sensory biology of ichthyosaurs. The large eyes of ichthyosaurs may be associated with enlarged optic lobes, and the enlarged

cerebellum may allow for advanced locomotory capabilities. The olfactory lobes are also enlarged, suggesting that olfaction may have played a larger role in the lives of ichthyosaurs than previously thought. Phylogenetic analysis places BRLSI M1399 within Thunnosauria, but with a mix of leptonectid characters and derived characters commonly found in ophthalmosaurs. It is evident that by the Toarcian, ichthyosaurs not only had osteological adaptations to life at sea, but also the neurological adaptations to be highly mobile predators, with acute vision and a developed sense of olfaction.

Acknowledgements. We thank Valentin Fischer for correspondence and advice, Andrew Cuff and David Button for training in Avizo and Richard Dearden for training in TNT. We thank Valentin Fischer, Davide Foffa and Sally Thomas for their detailed reviews and suggested corrections, which have all much improved the manuscript. In particular, we thank Remmert Schouten for his invaluable assistance in securing an excellent CT scan of the specimen, Lorie Barber for expert mechanical preparation and the Esmée Fairbairn Foundation for financial support for scanning and preparation work.

DATA ARCHIVING STATEMENT

Data and supporting information for this study are available in the Dryad Digital Repository: http://dx.doi.org/10.5061/dryad.gs340

Appendix S1. Phylogenetic methods.

Figure S1. Strict consensus of nine most parsimonious trees (146 steps) recovered using exact search on the matrix of Fischer *et al.* (2013) with BRLSI M1399 added as an additional taxon, and *Hauffiopteryx typicus* recoded to exclude this material.

Editor. Imran Rahman

REFERENCES

ANDREWS, C. W. 1910. *A descriptive catalogue of the marine reptiles of the Oxford Clay. Part I*. British Museum (Natural History), London, 205 pp.

APPLEBY, R. M. 1961. On the cranial morphology of ichthyosaurs. *Proceedings of the Zoological Society of London*, **137**, 333–370.

ARAÚJO, R. and POLCYN, M. J. 2013. A biomechanical analysis of the skull and adductor chamber muscles in the Late Cretaceous Plesiosaur *Libonectes*. *Palaeontologia Electronica*, **16**, 25.

BALANOFF, A. M., BEVER, G. S., ROWE, T. B. and NORELL, M. A. 2013. Evolutionary origins of the avian brain. *Nature*, **501**, 93–96.

BARDET, N. 1992. Stratigraphic evidence for the extinction of the ichthyosaurs. *Terra Nova*, **4**, 649–656.

BARTON, R. A. 2004. Binocularity and brain evolution in primates. *Proceedings of the National Academy of Sciences of the United States of America*, **101**, 10113–10115.

BENNETT, S. P., BARRETT, P. M., COLLINSON, M. E., MOORE-FAY, S., DAVIS, P. G. and PALMER, C. P. 2012. A new specimen of *Ichthyosaurus communis* from Dorset, UK, and its bearing on the stratigraphic range of the species. *Proceedings of the Geologists' Association*, **123**, 146–154.

BRUSATTE, S. L., BENTON, M. J., RUTA, M. and LLOYD, G. T. 2008. Superiority, competition, and opportunism in the evolutionary radiation of dinosaurs. *Science*, **321**, 1485–1488. doi:10.1126/science.1161833

BURTON, R. F. 2008. The scaling of eye size in adult birds: relationship to brain, head and body sizes. *Vision Research*, **48**, 2345–2351.

CAINE, H. and BENTON, M. J. 2011. Ichthyosauria from the Upper Lias of Strawberry Bank, England. *Palaeontology*, **54**, 1069–1093.

CUFF, A. R. and RAYFIELD, E. J. 2013. Feeding mechanics in spinosaurid theropods and extant crocodilians. *PLoS One*, **8**, e65295.

DRUCKENMILLER, P. S. and MAXWELL, E. E. 2010. A new Lower Cretaceous (lower Albian) ichthyosaur genus from the Clearwater Formation, Alberta, Canada. *Canadian Journal of Earth Sciences*, **47**, 1037–1053.

DUFFIN, C. J. 1978. The Bath Geological Collections. The importance of certain vertebrate fossils collected by Charles Moore: an attempt at scientific perspective. *Geological Curators Group Newsletter*, **2**, 59–67.

—— 1979. *Pelagosaurus* (Mesosuchia, Crocodilia) from the English Toarcian (Lower Jurassic). *Neues Jahrbuch für Geologie und Paläontologie, Monatsheft*, **1979**, 475–485.

FERNÁNDEZ, M. S. 1999. A new ichthyosaur from the Los Molles Formation (Early Bajocian), Neuquén Basin, Argentina. *Journal of Paleontology*, **73**, 677–681.

—— CARABAJAL, A. P., GASPARINI, Z. and DÍAZ, G. C. 2011. A metriorhynchid crocodyliform braincase from northern Chile. *Journal of Vertebrate Paleontology*, **31**, 369–377.

FISCHER, V., MASURE, E., ARKHANGELSKY, M. S. and GODEFROIT, P. 2011. A new Barremian (Early Cretaceous) ichthyosaur from Western Russia. *Journal of Vertebrate Paleontology*, **31**, 1010–1025.

—— MAISCH, M. W., NAISH, D., KOSMA, R., LISTON, J., JOGER, U., KRÜGER, F. J., PARDO PÉREZ, J., TAINSH, J. and APPLEBY, R. M. 2012. New ophthalmosaurid ichthyosaurs from the European Lower Cretaceous demonstrate extensive ichthyosaur survival across the Jurassic-Cretaceous boundary. *PLOS ONE*, **7**, e29234. doi:10.1371/journal.pone.0029234

—— APPLEBY, R. M., NAISH, D., LISTON, J., RIDING, J. B., BRINDLEY, S. and GODEFROIT, P. 2013. A basal thunnosaurian from Iraq reveals disparate phylogenetic origins for Cretaceous ichthyosaurs. *Biology Letters*, **9**, 20130021.

—— ARKHANGELSKY, M. S., USPENSKY, G. N., STENSHIN, I. M. and GODEFROIT, P. 2014. A new Lower Cretaceous ichthyosaur from Russia reveals skull shape conservatism within Ophthalmosaurinae. *Geological Magazine*, **151**, 60–70.

FOFFA, D., CUFF, A. R., SASSOON, J., RAYFIELD, E. J., MAVROGORDATO, M. N. and BENTON, M. J. 2014*a*. Functional anatomy and feeding biomechanics of a

giant Upper Jurassic pliosaur (Reptilia: Sauropterygia) from Weymouth Bay, Dorset, UK. *Journal of Anatomy*, **225**, 209–219.

—— SASSOON, J., CUFF, A. R., MAVROGORDATO, M. N. and BENTON, M. J. 2014*b*. Complex rostral neurovascular system in a giant pliosaur. *Naturwissenschaften*, **101**, 453–456.

FRÖBISCH, N. B., FRÖBISCH, J., SANDER, P. M., SCHMITZ, L. and RIEPPEL, O. 2013. Macropredatory ichthyosaur from the Middle Triassic and the origin of modern trophic networks. *Proceedings of the National Academy of Sciences of the United States of America*, **110**, 1393–1397.

GODEFROIT, P. 1993. The skull of *Stenopterygius longifrons* (Owen, 1881). *Revue de Paléobiologie, Volume Spéciale*, **7**, 1–18.

—— 1994. Les reptiles marins du Toarcien (Jurassique Inférieur) Belgo-Luxembourgeois. *Mémoirés pour server à l'Explication des Cartes Géoogiques et Miniéres de la Belgique*, **39**, 1–98.

GOLOBOFF, P. A., FARRIS, J. S., KÄLLERSJO, M., OXELMAN, B., RAMÍREZ, M. J. and SZUMIC, C. A. 2003. Improvements to resampling measures of group support. *Cladistics*, **19**, 324–332.

—— —— and NIXON K. C. 2008. TNT, a free program for phylogenetic analysis. *Cladistics*, **24**, 774–786.

HERRERA, Y. and VENNARI, V. V. 2015. Cranial anatomy and neuroanatomical features of a new specimen of Geosaurini (Crocodylomorpha: Metriorhynchidae) from west-central Argentina. *Historical Biology*, **27**, 33–41.

—— FERNÁNDEZ, M. S. and GASPARINI, Z. 2013. The snout of *Cricosaurus araucanensis*: a case study in novel anatomy of the nasal region of metriorhynchids. *Lethaia*, **46**, 331–340.

HOPSON, J. A. 1979. Paleoneurology. 39–146. *In* GANS, C., NORTHCUTT, R. G. and ULINSKY, P. (eds). *Biology of the Reptilia: 9 Neurology A*. Academic Press, London, 477 pp.

IWANIUK, A. N., HEESY, C. P., HALL, M. I. and WYLIE, D. R. W. 2008. Relative Wulst volume is correlated with orbit orientations and binocular visual field in birds. *Journal of Comparative Physiology, A*, **194**, 267–282.

KEAR, B. P. 2005. Cranial morphology of Platypterygius longmani Wade, 1990 (Reptilia: Ichthyosauria) from the Lower Cretaceous of Australia. *Zoological Journal of the Linnean Society*, **145**, 583–622.

KIRTON, A. M. 1983. *A review of British Upper Jurassic ichthyosaurs*. Unpublished PhD Thesis, University of Newcastle upon Tyne, Newcastle upon Tyne.

KOLB, C. and SANDER, P. M. 2009. Redescription of the ichthyosaur *Platypterygius hercynicus* (Kuhn 1946) from the Lower Cretaceous of Salzgitter (Lower Saxony, Germany). *Palaeontographica, Abteilung A*, **288**, 151–192.

LAUTENSCHLAGER, S. 2014. Palaeontology in the third dimension: a comprehensive guide for the integration of three-dimensional content in publications'. *Paläontologische Zeitschrift*, **88**, 111–121.

—— RAYFIELD, E. J., PERLE, A., ZANNO, L. J. and WITMER, L. M. 2012. The endocranial anatomy of Therizinosauria and its implications for sensory and cognitive function. *PLoS One*, **7**, e52289.

—— WITMER, L. M., PERLE, A. and RAYFIELD, E. J. 2013. Edentulism, beaks, and biomechanical innovations in the evolution of theropod dinosaurs. *Proceedings of the National Academy of Sciences of the United States of America*, **110**, 20657–20662.

MAISCH, M. W. 1997. Variationen im Verlauf der Gehirnnerven bei *Ophthalmosaurus* (Ichthyosauria, Jura). *Neues Jahrbuch für Geologie und Paläontologie, Monatshefte*, **1997**, 425–433.

—— 1998. A new ichthyosaur genus from the Posidonia Shale (Lower Toarcian, Jurassic) of Holzmaden, SW-Germany with comments on the phylogeny of post-Triassic ichthyosaurs. *Neues Jahrbuch für Geologie und Paläontologie, Abhandlungen*, **209**, 47–48.

—— 1999. Leptonectiden und Temnodontosauriden (Ichthyosauria) aus dem Alpha-Oelschiefer (Sinemurium) von Baden-Wuerttemberg (SW-Deutschland). *Neues Jahrbuch für Geologie und Paläontologie, Monatshefte*, **1999**, 490–512.

—— 2002. A braincase of *Temnodontosaurus* cf. *trigonodon* (von Theodori, 1843) (Ichthyosauria) from the Lower Jurassic of Germany. *Geologica et Palaeontololgica*, **36**, 115–122.

—— 2008. Revision der Gattung *Stenopterygius* Jaekel, 1904 emend. von Huene, 1922 (Reptilia: Ichthyosauria) aus dem unteren Jura Westeuropas. *Paleodiversity*, **1**, 227–271.

—— and MATZKE, A. T. 1997. *Mikadocephalus gracilirostris* n. gen., n. sp., a new ichthyosaur from the Grenzbitumenzone (Anisian–Ladinian) of Monte San Giorgio (Switzerland). *Paläontologische Zeitschrift*, **71**, 267–289.

—— —— 2000. The Ichthyosauria. *Stuttgarter Beiträge zu Naturkunde, Serie B, Geologie und Paläontologie*, **298**, 1–159.

—— —— 2003. The cranial osteology of the ichthyosaur *Leptonectes* cf. *tenuirostris* from the Lower Jurassic of England. *Journal of Vertebrate Paleontology*, **23**, 116–127.

—— —— 2006. The braincase of *Phantomosaurus neubigi* (Sander, 1997), an unusual ichthyosaur from the Middle Triassic of Germany. *Journal of Vertebrate Paleontology*, **26**, 598–607.

—— —— and BRINKMANN W. 2006. The otic capsule of the Middle Triassic ichthyosaur *Mixosaurus* from Monte San Giorgio (Switzerland): New evidence on the braincase structure of basal ichthyosaurs. *Eclogae Geologiae Helvetiae*, **99**, 205–210.

MAREK, R., MOON, B. C., WILLIAMS, M. and BENTON, M. J. 2015. Data from: The Skull and endocranium of a Lower Jurassic ichthyosaur based on digital reconstructions. *Dryad Digital Repository*. doi:10.5061/dryad.gs340

MARTIN, J. E., FISCHER, V., VINCENT, P. and SUAN, G. 2012. A longirostrine *Temnodontosaurus* (Ichthyosauria) with comments on Early Jurassic ichthyosaur niche partitioning and disparity. *Palaeontology*, **55**, 995–1005. doi:10.1111/j.1475-4983.2012.01159.x

MASSARE, J. A. 1987. Tooth morphology and prey preference of Mesozoic marine reptiles. *Journal of Vertebrate Paleontology*, **7**, 121–137.

MAXWELL, E. E. 2010. Generic reassignment of an ichthyosaur from the Queen Elizabeth Islands, Northwest Territories, Canada. *Journal of Vertebrate Paleontology*, **30**, 403–415.

—— FERNÁNDEZ, M. S. and SCHOCH, R. R. 2012. First diagnostic marine reptile remains from the Aalenian (Middle

Jurassic): a new ichthyosaur from southwestern Germany. *PLOS ONE*, **7**, e41692. doi:10.1371/journal.pone.0041692

MCGOWAN, C. 1973. The cranial morphology of the Lower Liassic latipinnate ichthyosaurs of England, *Bulletin of the British Museum (Natural History)*. *Geology*, **24**, 1–109.

—— 1989. Computed tomography reveals further details of *Excalibosaurus*, a putative ancestor for the swordfish-like ichthyosaur *Eurhinosaurus*. *Journal of Vertebrate Paleontology*, **9**, 269–281.

—— and MILNER, A. C. 1999. A new Pliensbachian ichthyosaur from Dorset, England. *Palaeontology*, **42**, 761–768.

—— and MOTANI, R. 2003. Part 8: Ichthyopterygia. 1–175. *In* SUES, H.-D. (ed.). *Handbook of Paleoherpetology*. Verlag Dr. Friedrich Pfeil, Munich, 175 pp.

MERRIAM, J. C. 1908. Triassic Ichthyosauria, with special reference to the American forms. *Memoirs of the University of California*, **1**, 1–252.

MOORE, C. 1866. On the Middle and Upper Lias of the South West of England. *Proceedings of the Somersetshire Archaeological and Natural History Society*, **13**, 119–244.

MOTANI, R. 2005. Evolution of fish-shaped reptiles (Reptilia: Ichthyopterygia) in their physical environments and constraints. *Annual Reviews of Earth and Planet Sciences*, **33**, 395–420.

—— ROTHSCHILD, B. M. and WAHL, W. 1999. Large eyeballs in diving ichthyosaurs. *Nature*, **402**, 747.

—— JI, C., TOMITA, T., KELLEY, N., MAXWELL, E. E., JIANG, D. Y. and SANDER, P. M. 2013. Absence of suction feeding ichthyosaurs and its implications for Triassic mesopelagic paleoecology. *PLoS One*, **8**, e66075.

NEENAN, J. M. and SCHEYER, T. M. 2012. The braincase and inner ear of *Placodus gigas* (Sauropterygia, Placodontia) – a new reconstruction based on computed tomographic data. *Journal of Vertebrate Paleontology*, **32**, 1350–1357.

NICHOLLS, E. L. and MANABE, M. 2004. Giant ichthyosaurs of the Triassic–a new species of *Shonisaurus* from the Pardonet Formation (Norian: Late Triassic) of British Columbia. *Journal of Vertebrate Paleontology*, **24**, 838–849.

NOMURA, T., KAWAGUCHI, M., ONO, K. and MURAKAMI, Y. 2013. Reptiles: a new model for brain evo-devo research. *Journal of Experimental Zoology, Part A*, **320**, 57–73.

OWEN, R. 1881. A monograph of the fossil Reptilia of the Liassic Formations. Part Third. *Ichthyosaurus. Monographs of the Palaeontographical Society*, **35**, 83–134.

PIERCE, S. and BENTON, M. J. 2006. *Pelagosaurus typus* Bronn, 1841 (Mesoeucrocodylia: Thalattosuchia) from the Upper Lias (Toarcian; Lower Jurassic) of Somerset, England. *Journal of Vertebrate Paleontology*, **26**, 621–635.

PORTER, K. R. 1972. *Herpetology*. W. B. Saunders, Philadelphia, 524 pp.

QUAY, W. B. 1979. The parietal eye-pineal complex. 245–406. *In* GANS, C., NORTHCUTT, R. G. and ULINSKY, P. (eds). *Biology of the Reptilia: 9 Neurology A*. Academic Press, London, 477 pp.

RAYFIELD, E. J. 2005. Aspects of comparative cranial mechanics in the theropod dinosaurs *Coelophysis*, *Allosaurus* and *Tyrannosaurus*. *Zoological Journal of the Linnean Society*, **144**, 309–316.

ROBERTS, A. J., DRUCKENMILLER, P. S., SÆTRE, G.-P. and HURUM, J. H. 2014. A new Upper Jurassic ophthalmosaurid ichthyosaur from the Slottsmøya Member, Agarhdfjellet Formation of central Spitsbergen. *PLoS One*, **9**, e103152.

ROGERS, S. W. 2005. Reconstructing the behaviors of extinct species: An excursion into comparative paleoneurology. *American Journal of Medical Genetics, A*, **134**, 349–356.

ROMER, A. S. 1968. An ichthyosaur skull from the Cretaceous of Wyoming. *Rocky Mountain Geology*, **7**, 27–41.

SANDER, P. M., CHEN, X., CHENG, L. and WANG, X. F. 2011. Short-snouted toothless ichthyosaur from China suggests Late Triassic diversification of suction feeding ichthyosaurs. *PLoS One*, **6**, e19480.

SATO, T., WU, X.-C., TIRABASSO, A. and BLOSKIE, P. 2011. Braincase of a polycotylid plesiosaur (Reptilia: Sauropterygia) from the Upper Cretaceous of Manitoba, Canada. *Journal of Vertebrate Paleontology*, **31**, 313–329.

SCHAEFFER, D. O. and WATERS, R. M. 1996. Neuroanatomy and neurological diseases of reptiles. *Seminars in Avian and Exotic Pet Medicine*, **5**, 165–171.

SLIJPER, E. J. 1962. *Whales*. Basic Books, New York, 475 pp.

SOLLAS, W. J. 1916. The skull of *Ichthyosaurus*, studied in serial sections. *Philosophical Transactions of the Royal Society, London, Series B*, **208**, 63–126.

TEN DONKELAAR, H. J. and BANGMA, G. C. 1979. The cerebellum. 496–586. *In* GANS, C. and ULINSKY, P. (eds). *Biology of the Reptilia: 17 Neurology C*. Academic Press, London, 790 pp.

THEWISSEN, J. G. M., GEORGE, J., ROSA, C. and KISHIDA, T. 2010. Olfaction and brain size in the bowhead whale (*Balaena mysticetus*). *Marine Mammal Science*, **27**, 282–294.

THORNE, P. M., RUTA, M. and BENTON, M. J. 2011. Resetting the evolution of marine reptiles at the Triassic-Jurassic boundary. *Proceedings of the National Academy of Sciences of the United States of America*, **108**, 8339–8344.

WEBB, P. W. and BUFFRÉNIL, V. de 1990. Locomotion in the biology of large aquatic vertebrates. *Transactions of the American Fisheries Society*, **119**, 629–641.

WROE, S., CHAMOLI, U., PARR, W. C. H., CLAUSEN, P., RIDGELY, R. and WITMER, L. M. 2013. Comparative biomechanical modeling of metatherian and placental saber-tooths: a different kind of bite for an extreme pouched predator. *PLoS One*, **8**, e66888.